(12) BS

(9) rept. nos. 3, 4 and 5 for period ending 15 Oct 75,

Technical Reports 3, 4, 5; October 15, 1975

#3 -- EFFECT OF THE MgO/SiO_2 RATIO ON THE STRENGTH OF HOT-PRESSED Si_3N_4.

(6) (10) C. A. Andersson, F. F. Lange and J. L. Iskoe

#4 -- INTERRELATION BETWEEN CREEP AND SLOW CRACK GROWTH.

F. F. Lange

#5 -- CRACK EXTENSION AND ARREST: THEORY AND EXPERIMENTS FOR CONTACT STRESS FIELDS.

F. F. Lange

Westinghouse Electric Corporation
Research and Development Center

(11) 15 Oct 75

(12) 48p.

Contract Number N00014-74-C-0284,

Sponsored by the Advanced Projects Agency
ARPA Order Number 2697
Program Code Number 01269

Scientific Officer: Dr. A. M. Diness
Office of Naval Research

Principal Investigator: Dr. F. F. Lange
(412) 256-3684

Effective Date of Contract: April 1, 1974

Contract Expiration Date: June 30, 1976

Amount of Contract: $159,892

Form Approved, Budget -- No. 22-R0293

376 625
607

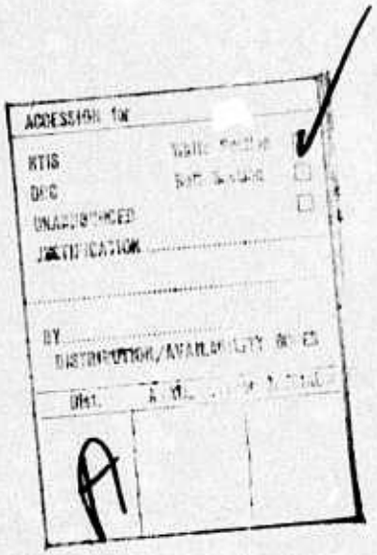
ACCESSION for
NTIS
DDC
UNANNOUNCED
JUSTIFICATION
BY
DISTRIBUTION/AVAILABILITY CODES
Dist.
A

EFFECT OF THE MgO/SiO_2 RATIO ON THE STRENGTH OF HOT-PRESSED Si_3N_4

Technical Report #3, October 15, 1975

Westinghouse Electric Corporation
Research and Development Center

Contract Number N00014-74-C-0284

Sponsored by the Advanced Projects Agency
ARPA Order Number 2697
Program Code Number 01269

Scientific Officer: Dr. A. M. Diness
Office of Naval Research

Principal Investigator: Dr. F. F. Lange
(412) 256-3684

Effective Date of Contract: April 1, 1974

Contract Expiration Date: June 30, 1976

Amount of Contract: $159,892

Form Approved, Budget -- No. 22-R0293

October 15, 1975

EFFECT OF THE MgO/SiO_2 RATIO ON THE STRENGTH OF HOT-PRESSED Si_3N_4

C. A. Andersson, F. F. Lange and J. L. Iskoe

Metallurgy and Metals Processing
Westinghouse Research Laboratories
Pittsburgh, Pennsylvania 15235

No. 3.

ABSTRACT

The strength of hot-pressed Si_3N_4 containing different MgO/SiO_2 molar ratios was studied. Significant increases in strength at 1400°C were observed as the MgO/SiO_2 ratio increased to 3-4. Smaller decreases in strength at both 25°C and 1400°C were observed when $MgO/SiO_2 > 4$. These observations are briefly discussed with regard to possible chemistry changes of the grain boundary phase believed to be present in hot-pressed Si_3N_4.

no. 4 p. 1

1. INTRODUCTION

Silicon nitride hot-pressed with the aid of MgO is believed to consist of β-Si_3N_4 grains separated by a silicate phase.[1] Impurities such as CaO have been shown to effect the mechanical properties at elevated temperatures by reducing the refractoriness of the grain boundary phase.[2] Recognizing that a significant improvement in these properties could be achieved by the reduction of such contaminants, a successful effort was made to produce higher purity starting powder at Westinghouse.

Once the overwhelming effect of impurities was radically reduced, a new effect was discovered. Chronologically, it was discovered that the high temperature strength was dependent on the amount of the

MgO hot-pressing aid used to densify a given starting powder as shown in Fig. 1. This unexpected effect was eventually rationalized by hypothesizing that the MgO/SiO_2 ratio* was the controlling factor in this apparent relation. As detailed below, this hypothesis was confirmed by testing materials fabricated with different MgO/SiO_2 ratios.

2. EXPERIMENTAL

2.1 Powders

Different Si_3N_4 powders were manufactured by nitriding Si powder with additions of 0.0, 1.0 and 3.0 wt/o SiO_2. The phase content of the resulting powders were 83-93% α-Si_3N_4, 17-7% β-Si_3N_4 and $\leq$ 1% Si as determined by X-ray diffraction analysis. No correlation could be made between the SiO_2 additions and these crystalline phases.

The oxygen content of representative powders was determined after nitriding with the inert gas fusion, thermoconductivity method. Several powders were also analyzed by neutron activation, courtesy of H. Priest, AMMRC. Figure 2 illustrates that the oxygen content of different batches of Si_3N_4 powder is a function of the SiO_2 added prior to nitriding. The oxygen content of the Si powder was 0.4-0.5 wt/o. Since the oxygen content of the Si powder is most likely due to a surface layer of SiO_2, and the increase in oxygen content was proportional to the SiO_2 added prior to nitriding it was assumed that the oxygen content after nitriding corresponded to the SiO_2 in the Si_3N_4 powder.** It should be noted that the molar content of the apparent SiO_2 ranged between 1.7 and 6.7 mole/o. Commercial Si_3N_4 powders can have significantly higher SiO_2 contents.[4]

---

* SiO_2 is a common contaminant in Si_3N_4 powders.[3,4]

** As recently shown by Kohatsu and McCauley[5] oxygen is not a necessary element of the α-Si_3N_4 structure as previously reported by Wild, et al.[6]

Table 1 reports the cation impurity content of the Si_3N_4 powders. No variation in impurity content outside of experimental error was observed between different batches.

Si_3N_4 powders containing different MgO/SiO_2 ratios were prepared by mixing 2-8 w/o MgO with Si_3N_4 powders containing different apparent SiO_2 contents. In addition, the MgO/SiO_2 ratio of several powders was also varied by mixing both MgO and SiO_2 into a powder with an oxygen content of 0.4 w/o (0.75 w/o SiO_2). Mixing and particle size reduction was performed by milling with methanol in polyethylene bottles using WC cylindrical grinding media. Oxygen analysis before and after milling showed no changes that could not be accounted for by the MgO addition.

2.2 Densification and Mechanical Testing

After stir-drying, the milled composite powders were hot-pressed in a N_2 atmosphere with a stress of 28 MN/m^2 at a temperature of 1750°C for 1-4 hrs to produce 5 cm diameter by 0.75 cm discs. The powders were separated from the graphite die with grafoil. Density was determined by water immersion.

Bar specimens (0.317 x 0.635 x 3.17 cm) were sectioned and ground with a 320 grit diamond wheel. Room temperature flexural strength measurements were made at a crosshead speed of 0.05 cm/min using a metal fixture (0.635 cm inner and 1.905 cm outer loading spans). Elevated temperature measurements were performed in air at 1400°C with a crosshead speed of 0.005 cm/min using a hot-pressed Si_3N_4 fixture (0.950 cm inner and 2.22 cm outer loading spans).

3. RESULTS

Densities varied between 3.20 gm/cc and 3.29 gm/cc due to a slight variation in the tungsten contamination during milling.

Flexural strength data at 25°C and 1400°C are shown in Fig. 3 as a function of the MgO/SiO_2 ratio. Each point, represented by a number indicating the weight % of the MgO hot-pressing aid, corresponds to the average result from a single billet (3-6 measurements at 25°C and 3 measurements at 1400°C). Because the oxygen content of only half of the Si_3N_4 powders were directly determined, the linear relation shown in Fig. 2 was used to calculate the oxygen content of the other powders. The oxygen content was used to calculate the apparent SiO_2 content and thus, the MgO/SiO_2 molar ratio. The circled numbers correspond to materials where SiO_2 was added to Si_3N_4 powder.

As shown, the strength at 25°C exhibits much scatter.* Mean values are 655 MN/m^2 for $MgO/SiO_2 \leq 4$, apparently decreasing to 520 MN/m^2 at $MgO/SiO_2 = 10$.

At 1400°C, the mean strength increases from 170 MN/m^2 at low MgO/SiO_2 ratios to 415 MN/m^2 at $MgO/SiO_2 = 3$ and then decreases to 345 MN/m^2 at higher MgO/SiO_2 ratios. The circled points should be noted since they represent results for materials where the MgO/SiO_2 ratio was lowered by adding SiO_2 to the starting Si_3N_4 powder. Without the additional SiO_2, the same Si_3N_4 powders had greater MgO/SiO_2 ratios and corresponding higher strengths.

Figure 4 illustrates load-deflection curves for selected specimens with different MgO/SiO_2 ratios, indicating that less non-elastic deformation occurs at $MgO/SiO_2 > 3$.

4. DISCUSSION

The increase in strength at 1400°C for $0 < MgO/SiO_2 \leq 4$ can be interpreted as due to a change in the grain boundary phase. Either a change in its refractoriness or its volume content would result in

* The observed scatter may have been due to the small differences in hot-pressing schedules, e.g., heating rates, mode of pressure application, etc., used by the 3 different investigators, which can influence the resulting microstructure and thus the fracture toughness and strength of hot-pressed Si_3N_4.[7]

lower rates for grain boundary separation and sliding,[8] thus decreasing the materials susceptibility to sub-critical crack growth and non-elastic deformation at high temperatures.[9]

The reason for the apparent decrease in strength at 25°C and 1400°C for $MgO/SiO_2 > 4$ requires further experiments. The authors believe that this effect is related to the volume content of the grain boundary phase, which might govern the material's grain structure.

The composition and volume fraction of the grain boundary phase are presently unknown. Oyama and Kamigaito[10] have reported data suggesting that up to 30 mole % of MgO is soluble in Si_3N_4. These investigators neglected the presence of the SiO_2 contamination in the Si_3N_4 powder; thus the real phase relations in the Si_3N_4-SiO_2-MgO-Mg_3N_2 system are presently unknown. In any case, Oyama and Kamigaito's results suggest that the MgO densification aid would be present in both the β-Si_3N_4 structure and the grain boundary phase.

A change in either the refractoriness or the volume content of the grain boundary can occur by shifting compositions with the Si_3N_4-SiO_2-MgO-Mg_3N_2 system, e.g., by shifting to a new phase field, the grain boundary phase may not be a silicate. On the other hand, the change in strength with the MgO/SiO_2 ratio may be a result of shifting away from glass forming regions in the MgO-SiO_2-impurity system, i.e., silicate composition containing large proportions of MgO are less apt to form glasses upon solidification. Phase equilibrium studies would clarify these different viewpoints.

5. CONCLUSION

It has been shown that the MgO/SiO_2 ratio has a significant effect on the high temperature strength of Si_3N_4. Thus optimum strengths can only be achieved by controlling extrinsic impurities, e.g., CaO, and the SiO_2 content of starting α-Si_3N_4 powders.

ACKNOWLEDGMENTS

The authors would like to acknowledge the technical assistance of J. J. Nalevanko, W. J. Carmen and J. P. Yex. This work was supported by the Advanced Projects Research Agency through the Office of Naval Research, Contract No. N00014-74-C-0284.

REFERENCES

1. F. F. Lange, "Strong, High-Temperature Ceramics", Ann. Rev. Mat. Sci. 4, 365 (1974).
2. J. L. Iskoe, F. F. Lange and E. S. Diaz, "Effect of Selected Impurities on the High Temperature Mechanical Properties of Hot-Pressed Si_3N_4", J. Mat. Sci. (in press).
3. I. Colquhoun, D. P. Thompson, W. I. Wilson, P. Grieveson and K. Jack, "Determination of Surface SiO_2 and Its Effect on the Hot-Pressing Behavior of α-Si_3N_4 Powder", Proc. Brit. Ceram. Soc. No. 22, 181 (1973).
4. F. F. Lange, "Task I: Fabrication, Microstructure and Selected Properties of SiAlON Compositions", Final Rept. NAVAIR Contract N00019-73-C-0208, February 1974.
5. I. Kohatsu and J. W. McCauley, "Re-Examination of the Crystal Structure of α-Si_3N_4", Mat. Res. Bull. 9, 917 (1974).
6. S. Wild, P. Grieveson and K. H. Jack, "Crystal Structures of α and β Si_3N_4 and Ge_3N_4", Special Ceramics, 5, Ed. by P. Popper, p. 385, B.C.R.A., Stoke-on-Trent (1974).
7. J. L. Iskoe and F. F. Lange, "Microstructural Development of Si_3N_4 Hot-Pressed with MgO", to be published.
8. F. F. Lange, "Non-Elastic Deformation of Polycrystals with a Liquid Boundary Phase", Deformation of Ceramic Materials, Ed. by R. C. Bradt and R. E. Tressler, p. 361, Plenum (1975).

9. F. F. Lange, "High-Temperature Strength Behavior of Hot-Pressed Si_3N_4: Evidence for Sub-Critical Crack Growth", J. Am. Ceram. Soc. 57, 84 (1974).

10. Y. O. Oyama and O. Kamigaito, "A Study on the Sintered Si_3N_4-MgO System", Yogyo-Kyokai-Shi 81, 34 (1973).

FIGURE CAPTIONS

FIG. 1 -- Flexural strength at 1400°C vs MgO content used for densification. Each point is an average of 3 specimens from a single billet. Test conditions are given in text. Oxygen content of different powders was 0.9-1.6 w/o.

FIG. 2 -- Oxygen content of Si_3N_4 powder vs SiO, added to Si powder prior to nitriding.

FIG. 3 -- Flexural strength vs MgO/SiO_2 molar ratio.

FIG. 4 -- Bending moment vs deflection for typical flexural specimens fabricated with different MgO/SiO_2 molar ratios.

Table 1

Spectrographic Analyses of Westinghouse Si_3N_4 Starting Powder (wt %)

Al		0.08
Ag	<	0.001
B		0.001
Ca		0.016
Cr		0.01
Fe	>	0.1
Mg		0.001
Mn		0.05
Mo	<	0.003
Ni	<	0.01
Pb	<	0.01
Sb	<	0.01
Sn	<	0.01
Ti		0.01
V		0.005
Zn	<	0.01

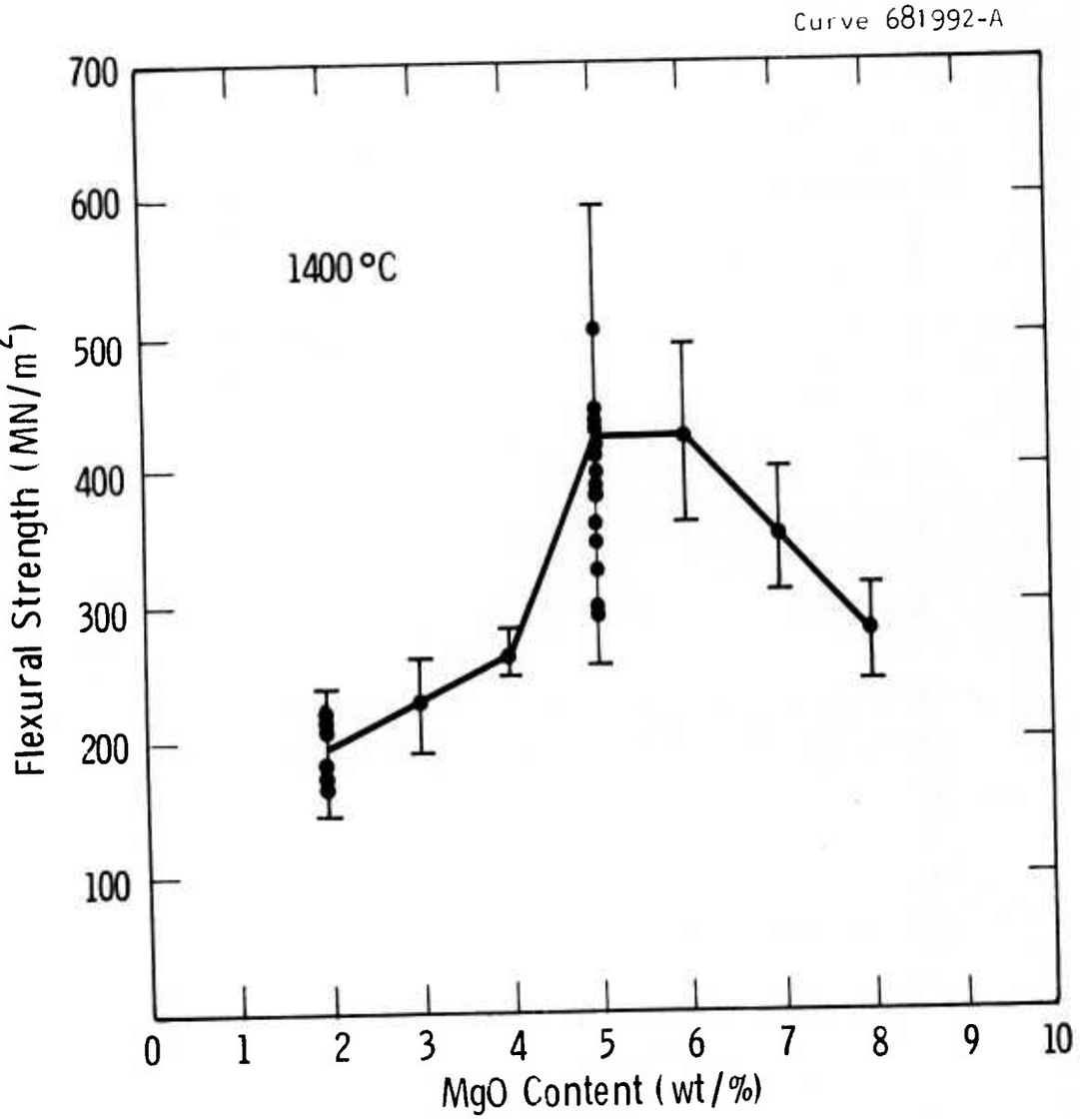
Curve 681992-A
700
600
500
400
300
200
100
1400 °C
Flexural Strength (MN/m^2)
0
1
2
3
4
5
6
7
8
9
10
MgO Content (wt/%)

Fig. 1

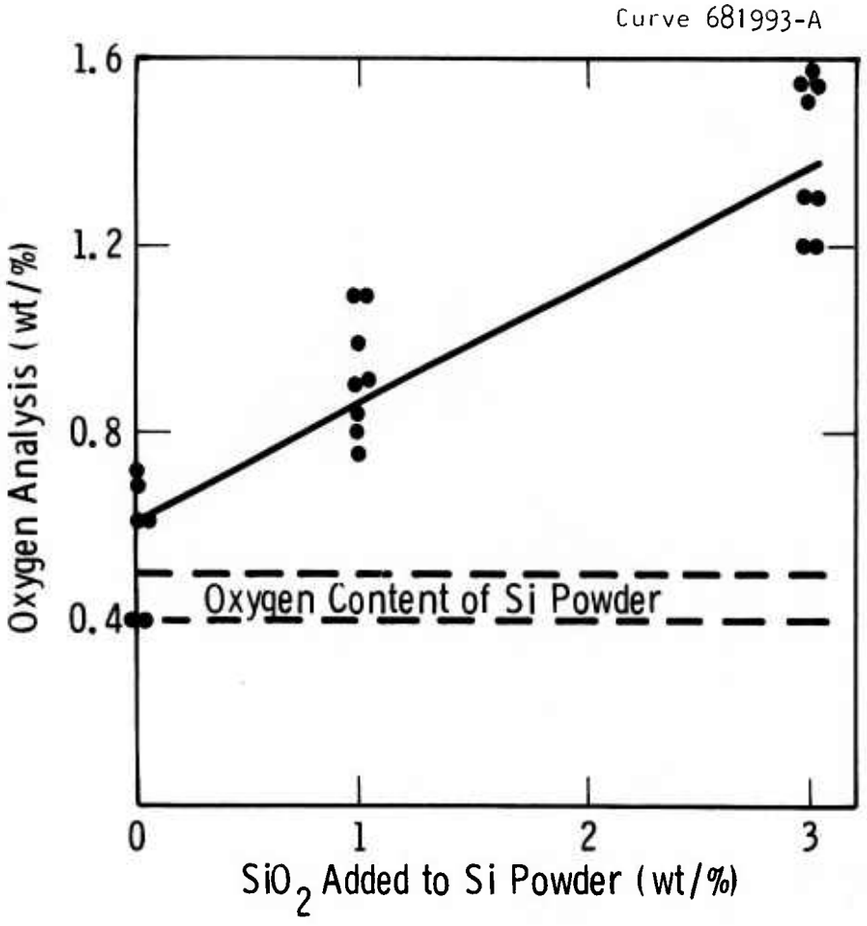
Curve 681993-A
1.6
1.2
0.8
0.4
Oxygen Analysis (wt/%)
Oxygen Content of Si Powder
0
1
2
3
SiO2 Added to Si Powder (wt/%)

Fig. 2

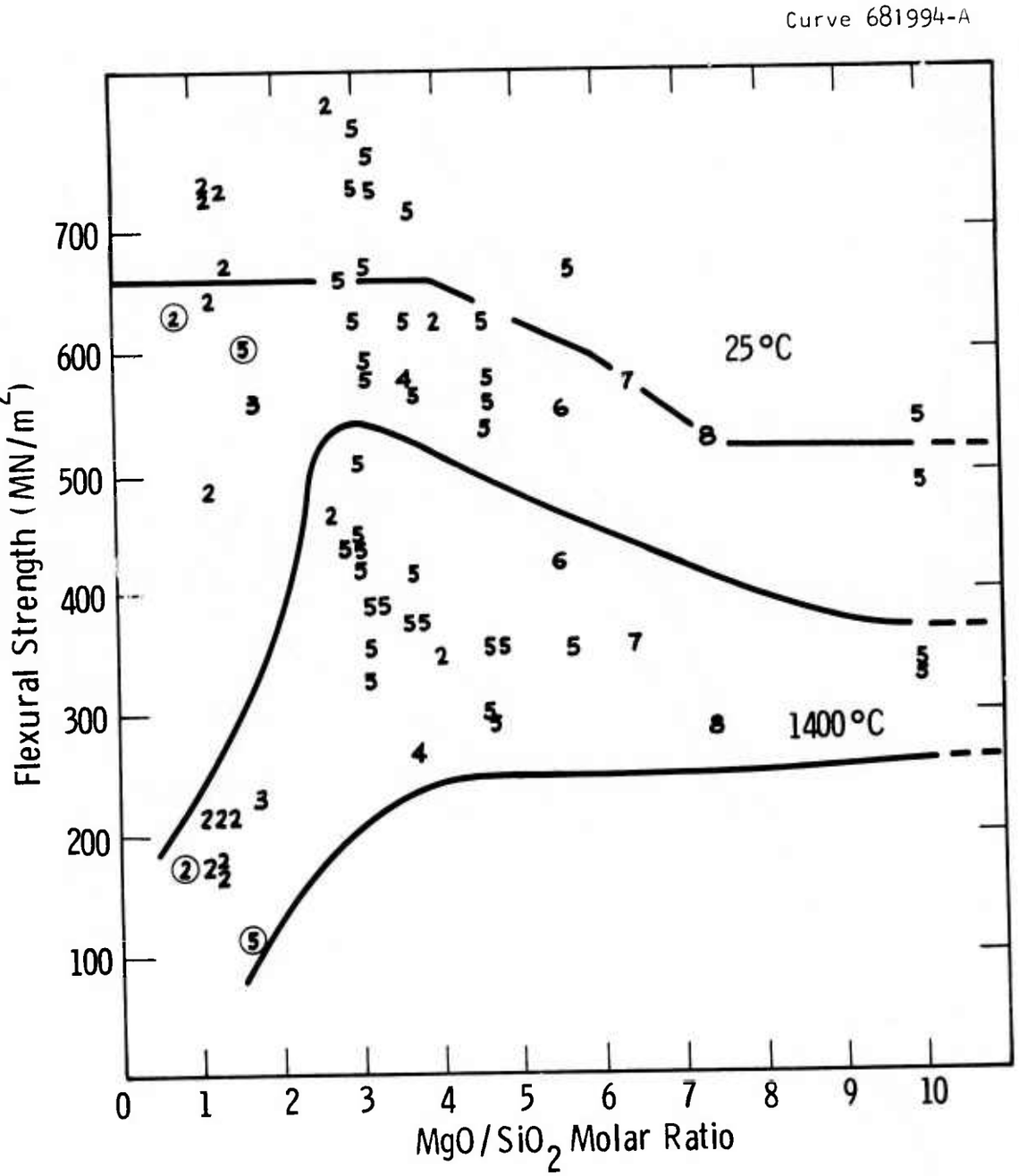
Curve 681994-A
Flexural Strength (MN/m^2)
700
600
500
400
300
200
100
25°C
1400°C
0
1
2
3
4
5
6
7
8
9
10
MgO/SiO$_2$ Molar Ratio

Fig. 3

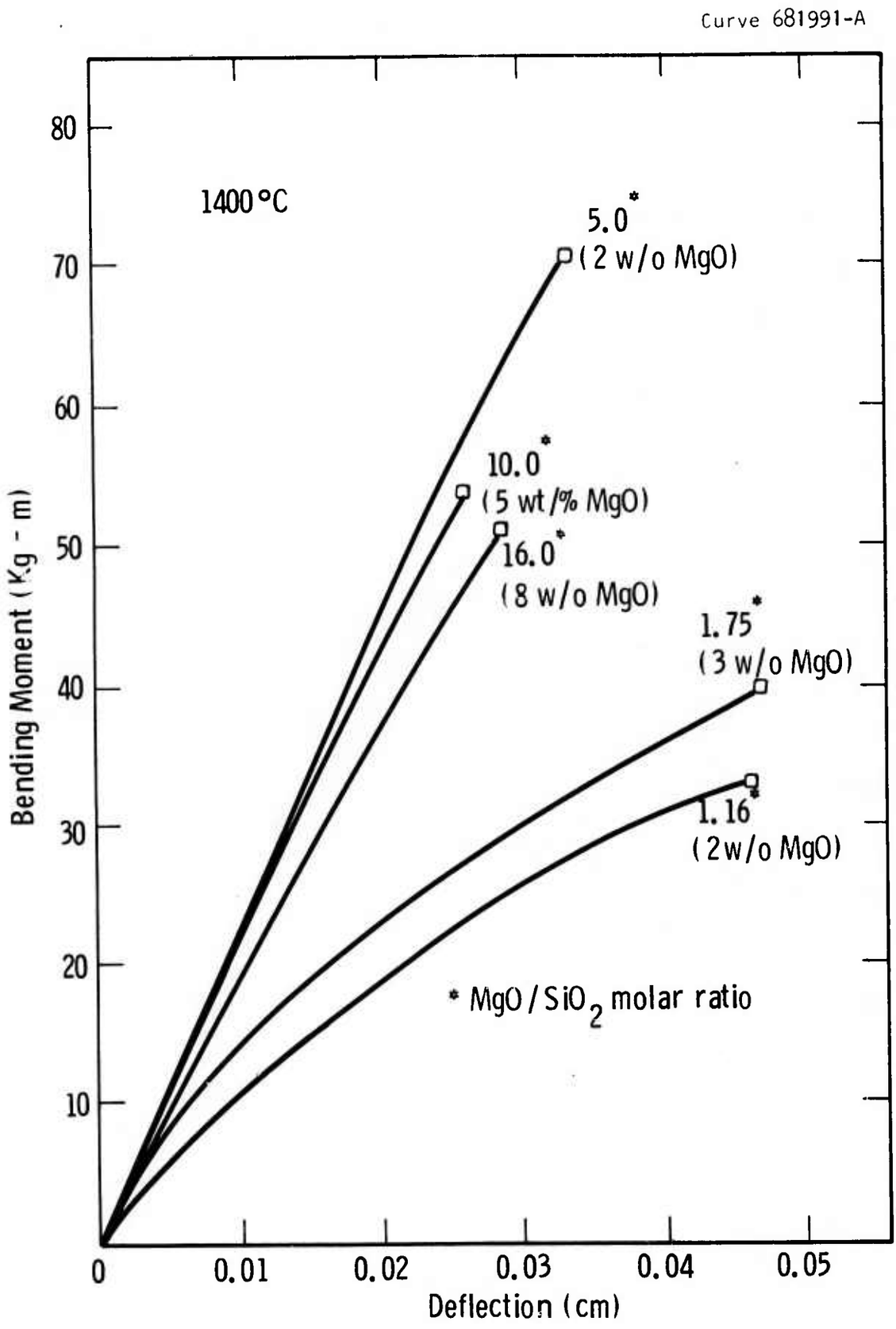
Curve 681991-A
1400°C
5.0*
(2 w/o MgO)
10.0*
(5 wt/% MgO)
16.0*
(8 w/o MgO)
1.75*
(3 w/o MgO)
1.16*
(2w/o MgO)
* MgO / SiO2 molar ratio
Bending Moment (Kg - m)
Deflection (cm)
80
70
60
50
40
30
20
10
0
0.01
0.02
0.03
0.04
0.05

Fig. 4

Unclassified

Security Classification

#3

DOCUMENT CONTROL DATA - R&D

(Security classification of title, body of abstract and indexing annotation must be entered when the overall report is classified)

1. ORIGINATING ACTIVITY *(Corporate author)*

Westinghouse Research & Development Center
Pittsburgh, PA 15235

2a. REPORT SECURITY CLASSIFICATION

Unclassified

2b. GROUP

3. REPORT TITLE

EFFECT OF THE MgO/SiO_2 RATIO ON THE STRENGTH OF HOT-PRESSED Si_3N_4

4. DESCRIPTIVE NOTES *(Type of report and inclusive dates)*

5. AUTHOR(S) *(Last name, first name, initial)*

Andersson, C. A., Lange, F. F. and Iskoe, J. L.

6. REPORT DATE

October 15, 1975

7a. TOTAL NO. OF PAGES

7b. NO. OF REFS

8a. CONTRACT OR GRANT NO.

N00014-74-C-0284

b. PROJECT NO.

c.

d.

9a. ORIGINATOR'S REPORT NUMBER(S)

9b. OTHER REPORT NO(S) *(Any other numbers that may be assigned this report)*

None

10. AVAILABILITY/LIMITATION NOTICES

Reproduction in whole or in part is permitted for any purpose of the U. S. Government. Distribution of this document is UNLIMITED.

11. SUPPLEMENTARY NOTES

12. SPONSORING MILITARY ACTIVITY

Advanced Research Projects Agency

13. ABSTRACT

The strength of hot-pressed Si_3N_4 containing different MgO/SiO_2 molar ratios was studied. Significant increases in strength at 1400°C were observed as the MgO/SiO_2 ratio increased 3-4. Smaller decreases in strength at both 25°C and 1400°C were observed when $MgO/SiO_2 > 4$. These observations are briefly discussed with regard to possible chemistry changes of the grain boundary phase believed to be present in hot-pressed Si_3N_4.

DD FORM 1 JAN 64 1473

Unclassified

Security Classification

RM 35054

14 KEY WORDS	LINK A		LINK B		LINK C	
	ROLE	WT	ROLE	WT	ROLE	WT
silicon nitride						
hot						
fabrication						
strength						
creep						
boundaries						
phase						
pressing						
grains						
equilibrium						

INSTRUCTIONS

1. ORIGINATING ACTIVITY: Enter the name and address of the contractor, subcontractor, grantee, Department of Defense activity or other organization *(corporate author)* issuing the report.

2*a*. REPORT SECURITY CLASSIFICATION: Enter the overall security classification of the report. Indicate whether "Restricted Data" is included. Marking is to be in accordance with appropriate security regulations.

2*b*. GROUP: Automatic downgrading is specified in DoD Directive 5200.10 and Armed Forces Industrial Manual. Enter the group number. Also, when applicable, show that optional markings have been used for Group 3 and Group 4 as authorized.

3. REPORT TITLE: Enter the complete report title in all capital letters. Titles in all cases should be unclassified. If a meaningful title cannot be selected without classification, show title classification in all capitals in parenthesis immediately following the title.

4. DESCRIPTIVE NOTES: If appropriate, enter the type of report, e.g., interim, progress, summary, annual, or final. Give the inclusive dates when a specific reporting period is covered.

5. AUTHOR(S): Enter the name(s) of author(s) as shown on or in the report. Enter last name, first name, middle initial. If military, show rank and branch of service. The name of the principal author is an absolute minimum requirement.

6. REPORT DATE: Enter the date of the report as day, month, year; or month, year. If more than one date appears on the report, use date of publication.

7*a*. TOTAL NUMBER OF PAGES: The total page count should follow normal pagination procedures, i.e., enter the number of pages containing information.

7*b*. NUMBER OF REFERENCES: Enter the total number of references cited in the report.

8*a*. CONTRACT OR GRANT NUMBER: If appropriate, enter the applicable number of the contract or grant under which the report was written.

8*b*, 8*c*, & 8*d*. PROJECT NUMBER: Enter the appropriate military department identification, such as project number, subproject number, system numbers, task number, etc.

9*a*. ORIGINATOR'S REPORT NUMBER(S): Enter the official report number by which the document will be identified and controlled by the originating activity. This number must be unique to this report.

9*b*. OTHER REPORT NUMBER(S): If the report has been assigned any other report numbers *(either by the originator or by the sponsor)*, also enter this number(s).

10. AVAILABILITY/LIMITATION NOTICES: Enter any limitations on further dissemination of the report, other than those imposed by security classification, using standard statements such as:

(1) "Qualified requesters may obtain copies of this report from DDC."

(2) "Foreign announcement and dissemination of this report by DDC is not authorized."

(3) "U. S. Government agencies may obtain copies of this report directly from DDC. Other qualified DDC users shall request through _____."

(4) "U. S. military agencies may obtain copies of this report directly from DDC. Other qualified users shall request through _____."

(5) "All distribution of this report is controlled. Qualified DDC users shall request through _____."

If the report has been furnished to the Office of Technical Services, Department of Commerce, for sale to the public, indicate this fact and enter the price, if known.

11. SUPPLEMENTARY NOTES: Use for additional explanatory notes.

12. SPONSORING MILITARY ACTIVITY: Enter the name of the departmental project office or laboratory sponsoring *(paying for)* the research and development. Include address.

13. ABSTRACT: Enter an abstract giving a brief and factual summary of the document indicative of the report, even though it may also appear elsewhere in the body of the technical report. If additional space is required, a continuation sheet shall be attached.

It is highly desirable that the abstract of classified reports be unclassified. Each paragraph of the abstract shall end with an indication of the military security classification of the information in the paragraph, represented as *(TS)*, *(S)*, *(C)*, or *(U)*.

There is no limitation on the length of the abstract. However, the suggested length is from 150 to 225 words.

14. KEY WORDS: Key words are technically meaningful terms or short phrases that characterize a report and may be used as index entries for cataloging the report. Key words must be selected so that no security classification is required. Identifiers, such as equipment model designation, trade name, military project code name, geographic location, may be used as key words but will be followed by an indication of technical context. The assignment of links, rules, and weights is optional.

INTERRELATION BETWEEN CREEP AND SLOW CRACK GROWTH

Technical Report #4, October 15, 1975

Westinghouse Electric Corporation
Research and Development Center

Contract Number N00014-74-C-0284

Sponsored by the Advanced Projects Agency
ARPA Order Number 2697
Program Code Number 01269

Scientific Officer: Dr. A. M. Diness
Office of Naval Research

Principal Investigator: Dr. F. F. Lange
(412) 256-3684

Effective Date of Contract: April 1, 1974

Contract Expiration Date: June 30, 1976

Amount of Contract: $159,892

Form Approved, Budget -- No. 22-R0293

October 15, 1975

INTERRELATIONS BETWEEN CREEP AND SLOW CRACK GROWTH

F. F. Lange

Metallurgy and Metals Processing
Westinghouse Research Laboratories
Pittsburgh, Pennsylvania 15235

ABSTRACT

No. 4 . Phenomenological interrelations between creep strain and slow crack growth are derived based on the fact that the total creep strain at fracture is determined by the growth kinetics of a pre-existing crack. It is shown that measurements of the creep strain in a region remote from the growing crack can be used to predict failure periods for materials that concurrently exhibit creep and slow crack growth.

no. 5, 6

1. INTRODUCTION

Certain materials have been found to concurrently exhibit creep and slow crack growth. Examples are discalloy,[1] AISI-4340 tempered steel,[2] glass-ceramics[3] and hot-pressed Si_3N_4.[4] For a given material and condition, both phenomenon can be governed by the same mechanism, e.g., grain boundary separation and sliding is the mechanism governing both creep and slow crack growth in polycrystals with a viscous grain boundary phase.[5] Or, both phenomenon can be governed by different mechanisms, e.g., creep, by dislocation movement and slow crack growth, by an environmental, stress-corrosion mechanism.

Usually creep and slow crack growth are treated independently. That is, creep laws are obtained for a material to define non-elastic strain as a function of stress and time and slow crack growth behavior is obtained from crack velocity-stress intensity relations that are used to predict failure time as a function of stress history. The purpose of this article is to show that these independently measured laws are interrelated regardless of the mechanism that control either phenomenon. It will be shown that the total strain at failure depends on the stress laws governing both phenomenon and that a measurement of strain and/or strain rate can be used to predict the failure time due to slow crack growth.

2. ANALYSIS OF INTERRELATION

It is assumed that a body under stress (σ_a) simultaneously exhibits non-elastic strain (creep) and slow crack growth. Also, for simplicity, it is assumed* that the creep strain can be described by

$$\varepsilon = \varepsilon_o + A\,\sigma_a^{\,n}\,t, \tag{1}$$

and that slow crack growth can be described by the crack velocity (v) - stress intensity factor (K) relation

$$v = B\,K^m, \tag{2}$$

where ε_o, A, n, B, and m are constants at a given temperature. The constants A and B contain the temperature dependent factors. The stress intensity factor can be stated in terms of the applied stress (σ_a), the crack size (c) and the dimensionless constant (Y) as

$$K = Y\,\sigma_a\,\sqrt{c}\ . \tag{3}$$

* The general concept would also apply for more complex laws, but the detailed results would be different.

Substituting Eq. (3) into Eq. (2),

$$v = \frac{dc}{dt} = B\, Y^m\, \sigma^m\, c^{m/2} \quad . \tag{4}$$

The total period of creep is limited to the time taken by the initial crack of size c_i to grow and cause failure. This failure time (t_f) is found by integrating Eq. (4) and assuming that $c_i^{2-m/2} >> c_f^{2-m/2}$ (c_f = crack size at failure):

$$t_f = \frac{2\, c_i^{2-m/2}}{(m-2)\, B\, Y^m}\, \sigma_a^{-m} \tag{5}$$

By substituting Eq. (5) into Eq. (1), the non-elastic strain at failure* (ε_f) is

$$\varepsilon_f = \varepsilon_o + \frac{2\, c_i^{(2-m)/2}}{(m-2)\, Y^m} \left(\frac{A}{B}\right) \sigma_a^{n-m} \tag{6}$$

This equation relates the stress dependencies of creep and slow crack growth to the creep strain at failure.

Likewise the failure time can be related to the steady state creep rate ($\dot{\varepsilon} = A\, \sigma_a^n$) by rearranging Eq. (5) and substituting for the stress

$$t_f = A^{m/n} \left(\frac{2\, c_i^{(2-m)/2}}{(m-2)\, B\, Y^m}\right) \dot{\varepsilon}^{-m/2} \tag{7}$$

In this equation, creep and slow crack growth are interrelated in terms of creep rate and failure time.

---

* Since Eq. (1) is derived from steady state creep data, Eq. (6) neglects the strain during tertiary creep.

3. DISCUSSION

3.1 The Extrinsic Parameters, c_i and Y

Equations (6) and (7) show the interrelation between creep and slow crack growth. Both equations were derived by substituting the applied stress-time to failure relation obtained from a fracture mechanics analysis into the commonly used relations to define creep strain. Both equations contain the intrinsic material parameters that define creep strain, viz., ε_o, A and n, and those that define the fracture mechanics of slow crack growth, viz., B and m. The two extrinsic parameters are the size of the initial pre-existing crack, c_i and the dimensionless constant, Y.

A problem arises concerning the size of the pre-existing crack when the analysis as summarized in Eqs. (6) and (7) is applied to either ductile (metals) or brittle (e.g., ceramics) materials. With regard to metals, the analysis assumes that a crack pre-exists prior to stressing. It is a common opinion among experimentalists investigating the creep of metals that cracks do not pre-exist in metal specimens, but they form after a period of extensive creep strain. The analysis is, therefore, not applicable for this case. On the other hand, the analysis does apply to large metal structures containing large pre-existing cracks, large flaws in castings, welded plates, etc.

Cracks pre-exist in most ceramics. Their distribution of sizes are responsible for the wider distribution of strength values for ceramics relative to metals.[6] Unfortunately, because the sizes of pre-existing cracks in most ceramics are small, techniques do not presently exist to determine their location and to measure their size. The problem of measuring the initial crack size for ceramics can be circumvented by using either the distribution of strength values to define the distribution of crack sizes or by truncating the distribution of crack sizes with a proof test. These two approaches are used in the Appendix to rederive both Eqs. (6) and (7).

A third approach to circumvent the crack size measurement is to simply use the mean strength value to define the mean crack size:

$$\bar{c}_i = \frac{K_c^2}{Y^2 \bar{\sigma}^2} , \tag{8}$$

where $\bar{\sigma}$ is the mean strength of the material obtained under conditions were slow crack growth does not occur.* K_c is the critical stress intensity factor.

Substituting Eq. (8) into Eqs. (6) and (7), one obtains the expressions relating the mean non-elastic strain at failure to the applied stress:

$$\bar{\varepsilon}_f = \varepsilon_o + \frac{2}{(m-2)\ Y^2} \left(\frac{\bar{\sigma}}{K_c}\right)^{(m-2)} \left(\frac{A}{B}\right) \sigma_a^{n-m} \tag{9}$$

and relating the mean failure time to the creep rate:

$$\bar{t}_f = A^{m/n} \left(\frac{2}{(m-2)\ Y^2\ B}\right) \left(\frac{\bar{\sigma}}{K_c}\right)^{(m-2)} \dot{\varepsilon}^{-m/2} \tag{10}$$

The value of the dimensionless parameter Y depends on the geometry of the crack (location, shape and size), the size of the crack relative to the size of the body and the stress distribution. For many conditions of tensile loading, $\sqrt{\pi} \leq Y \leq 2\sqrt{\pi}$.[7]

3.2 Temperature Dependence

The parameters A and B express the temperature dependence of creep and slow crack growth, respectively. Assuming activated processes, $A = A_o\ e^{-Qc/RT}$ and $B = B_o\ e^{-Qcg/RT}$, where Q_c = the activation

* For example, if slow crack growth is caused by a corrosive ambient, $\bar{\sigma}$ is obtained by measuring strengths in a non-corrosive ambient. Also, $\bar{\sigma}$ can be obtained by measuring strengths using very high loading rates to minimize the effect of slow crack growth on strength and thus, the calculation of the initial crack size.

energy for creep and Q_{cg} = the activation energy for crack growth. A_o and B_o are temperature and stress independent.

If the same phenomenon governs both creep and slow crack growth, the temperature dependence for both will be the same, e.g., $Q_c = Q_{cg}$. For this case, it can be seen by examining Eqs. (9) and (10) that the relation between ε_f and σ_a will be independent of temperature, whereas t_f vs $\dot{\varepsilon}$ will be temperature dependent.

3.3 Use of Interrelations

Linear representations for Eq. (9) and (10) can be obtained by taking logarithms. The graphical representations of log ε_f vs log σ_a will have a slope of (n-m) and log t_f vs log $\dot{\varepsilon}$ will have a slope of -m/n, (see Fig. 1).

From a scientific viewpoint, data plotted in this manner can be instructive for determining whether or not slow crack growth is responsible for failure and for determining the stress exponents for either creep or slow crack growth. For example, m > n for most materials, thus a negative slope for the log ε_f vs log σ_a strongly suggests that slow crack growth is responsible for failure. If one of the stress exponents is known, the other can be calculated from the relation: slope = n-m. Also, it can be strongly inferred that the same mechanism is responsible for both creep and slow crack growth if the log ε_f vs log σ_a is independent of temperature.

From an engineering viewpoint, the above analysis shows that strain measurements can be used to predict failure times for materials that concurrently creep and exhibit slow crack growth.* This is easily illustrated for a component subjected to a constant load at a fixed temperature. (1) The elastic portion of the measured strain determines

* It should be noted that this analysis also is true for two different materials, one exhibiting creep and the other exhibiting slow crack growth, joined in a series arrangement and subjected to the same load. Strain measurements on the material that creeps can be used to predict failure of the material exhibiting slow crack growth.

the applied stress which, in turn, is used to determine the non-elastic strain at failure from either Eq. (9) or a graphical log ε_f vs log σ_a plot. When the non-elastic strain approaches ε_f, the component is removed from service. (2) the measured creep rate ($\dot{\varepsilon}$) is used to calculate the failure period (t_f) using either Eq. (10) or a graphical log t_f vs log $\dot{\varepsilon}$ plot. The component is removed from service prior to the calculated failure period.

Likewise, but not as simple, failure strains and failure periods can be predicted from strain measurements for components subjected to conditions where both the load and the temperature are a function of time.

REFERENCES

1. J. D. Landes and J. A. Begley, ASTM STP 590, in press (1974).
2. J. D. Landes and R. P. Wei, ASME Pub. 73-MAT-B (1973).
3. R. Morrell and K. H. G. Ashbee, J. Mat. Sci. 8, 1253 (1973).
4. F. F. Lange, J. Am. Ceram. Soc. 57, 84 (1974).
5. F. F. Lange, Deformation of Ceramic Materials, Ed. R. C. Bradt and R. E. Tressler, p. 361, Plenum (1975).
6. W. Weibull, J. Appl. Mech. 18, 293 (1951).
7. A. S. Tetelman and A. G. Evans, Fracture Mechanics of Ceramics, Ed. R. C. Bradt, D. P. H. Hasselman and F. F. Lange, p. 898, Plenum (1974).
8. G. J. DeSalvo, Theory and Structural Design Applications of Weibull Statistics, Rep. WANL-TME 2688, Westinghouse Electric Corp., Astronuclear Laboratory (1970).
9. A. G. Evans and S. M. Wiederhorn, Intl. J. Fracture (in press).

APPENDIX

1. Creep-Crack Growth Interrelation Combined with Strength Statistics

The strength (σ_c) probability of failure (P) relation of a material containing a distribution of crack sizes can be expressed as[6]

$$P = 1\text{-}\exp\left[-\int \left(\frac{\sigma_c}{\sigma_o}\right)^w dV\right] \tag{1A}$$

where w and σ_o (Weibull's modulus and a normalizing stress, respectively) are material constants; V is the volume of the specimen or component. For certain stressing modes - component configurations,[8]

$$\int_V \left(\frac{\sigma}{\sigma_o}\right)^w dV = LV \left(\frac{\sigma}{\sigma_o}\right)^w , \tag{2A}$$

where L is a loading factor, e.g., for pure tension, L = 1.0. Thus, Eq. (1A) can be rewritten as

$$P = 1\text{-}\exp\left[-LV \left(\frac{\sigma}{\sigma_o}\right)^w\right]. \tag{3A}$$

Substituting into this equation the expression relating strength to crack size,

$$\sigma_c = \frac{K_c}{Y\, c_i^{1/2}} ,$$

one can obtain[9]

$$c_i = \left[\frac{\ell n \left(\frac{1}{1-P}\right)}{LV}\right]^{-2/w} \left(\frac{K_c}{\sigma_o Y}\right)^2 . \tag{4A}$$

Substituting Eq. (4A) into Eqs. (6) and (7) of the text, one obtains

$$\varepsilon_f = \varepsilon_o + \frac{2}{(m-2)\, Y^2} \left[\frac{\ell n \left(\frac{1}{1-P}\right)}{LV}\right]^{\frac{m-2}{w}} \left(\frac{\sigma_o}{K_c}\right)^{m-2} \left(\frac{A}{B}\right) \sigma_a^{n-m} \tag{5A}$$

and

$$t_f = \frac{2\,A^{m/n}}{(m-2)\,Y^2\,B}\left[\frac{\ell n\,(\frac{1}{1-P})}{LV}\right]^{\frac{m-2}{w}}\left(\frac{\sigma_o}{K_c}\right)^{m-2}\dot{\varepsilon}^{-m/n} \qquad (6A)$$

2. Creep-Crack Growth Interrelations Combined with Proof Testing

The maximum crack size in a component that survives an overload proof stress* (i.e., $\sigma_p > \sigma_a$, where $R = \sigma_p/\sigma_a$) is[9]

$$(c_i)_{max} = \left(\frac{K_c}{Y\,\sigma_p}\right)^2 \leq \left(\frac{K_c}{Y\,R\,\sigma_a}\right)^2 . \qquad (7A)$$

Substituting Eq. (7A) into Eqs. (6) and (7) of the text, one obtains a relation for the minimum** creep strain at failure:

$$\varepsilon_f \geq (\varepsilon_f)_{min} = \varepsilon_o + \frac{2}{(m-2)\,Y^2}\left(\frac{R}{K_c}\right)^{m-2}\left(\frac{A}{B}\right)\sigma_a^{n-2} \qquad (8A)$$

and the minimum** failure time:

$$t_f \geq (t_f)_{min} = \frac{2\,A^{m/n}}{(m-2)\,Y^2\,B}\left(\frac{R\,\sigma_a}{K_c}\right)^{m-2}\dot{\varepsilon}^{-m/n} \qquad (9A)$$

3. Graphical Representation of Resulting Expressions

As discussed in the text, Eqs. (5A), (6A), (8A) and (9A) can be graphically represented as log-log plots to facilitate the assessment of reliability. The log-log plots formed by these equations are a family of parallel lines shown by the following example for Eqs. (6A and 9A):

$$\log t_f = \log\left[\frac{2\,A^{m/n}}{(m-2)\,Y^2\,B}\left(\frac{\sigma_o}{K_c}\right)^{m-2}\right] + \frac{m-2}{w}\log\left[\frac{\ell n\,(\frac{1}{1-P})}{LV}\right] - \frac{m}{n}\log\dot{\varepsilon}$$

and

$$\log (t_f)_{min} = \log\left[\frac{2\,A^{m/n}}{(m-2)\,Y^2\,B}\left(\frac{\sigma_a}{K_c}\right)^{m-2}\right] + (m-2)\log R - \frac{m}{n}\log\dot{\varepsilon}$$

---

* The same stress distribution must exist in proof testing as in service.

** Proof testing only defines the largest possible crack and thus the minimum failure period (and thus, the minimum creep strain at failure).

Plotting these equations as log t_f (or log $(t_f)_{min}$) vs log $\dot{\varepsilon}$:

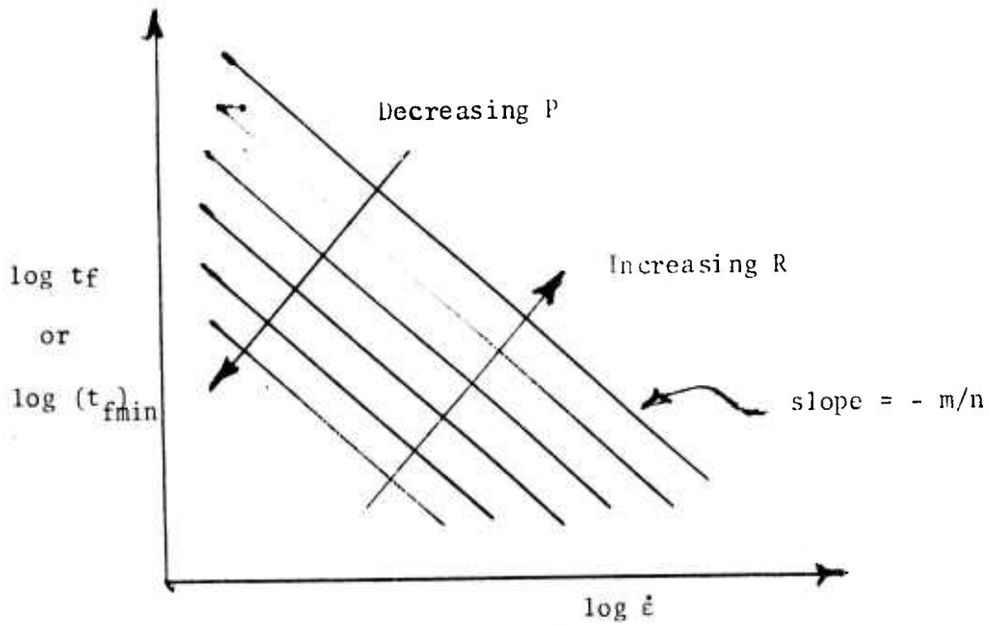

Fig. 1

These plots are used as follows. For a strain rate measured after a given period of service, the failure time is located on the graph either for a chosen probability of failure, P or, if the component had been proof tested prior to service, for the proof test ratio, R. The remaining service time is then calculated by subtracting the current service time from the failure time.

Unclassified
Security Classification

DOCUMENT CONTROL DATA - R&D

(Security classification of title, body of abstract and indexing annotation must be entered when the overall report is classified)

1. ORIGINATING ACTIVITY *(Corporate author)*
Westinghouse Research & Development Center
Pittsburgh, PA 15235

2a. REPORT SECURITY CLASSIFICATION
Unclassified

2b. GROUP

3. REPORT TITLE
INTERRELATION BETWEEN CREEP AND SLOW CRACK GROWTH

4. DESCRIPTIVE NOTES *(Type of report and inclusive dates)*

5. AUTHOR(S) *(Last name, first name, initial)*
Lange, F. F.

6. REPORT DATE
October 15, 1975

7a. TOTAL NO. OF PAGES

7b. NO. OF REFS

8a. CONTRACT OR GRANT NO.
N00014-74-C-0284

b. PROJECT NO.

c.

d.

9a. ORIGINATOR'S REPORT NUMBER(S)

9b. OTHER REPORT NO(S) *(Any other numbers that may be assigned this report)*
None

10. AVAILABILITY/LIMITATION NOTICES
Reproduction in whole or in part is permitted for any purpose of the U. S. Government. Distribution of this document is UNLIMITED.

11. SUPPLEMENTARY NOTES

12. SPONSORING MILITARY ACTIVITY
Advanced Research Projects Agency

13. ABSTRACT

Phenomenological interrelations between creep strain and slow crack growth are derived based on the fact that the total creep strain at fracture is determined by the growth kinetics of a pre-existing crack. It is shown that measurements of the creep strain in a region remote from the growing crack can be used to predict failure periods for materials that concurrently exhibit creep and slow crack growth.

DD FORM 1 JAN 64 1473

Unclassified
Security Classification

RM 35054

Unclassified

Security Classification

14 KEY WORDS	LINK A		LINK B		LINK C	
	ROLE	WT	ROLE	WT	ROLE	WT
creep						
slow						
fatigue						
failures						
cracks						
growth						

INSTRUCTIONS

1. ORIGINATING ACTIVITY: Enter the name and address of the contractor, subcontractor, grantee, Department of Defense activity or other organization *(corporate author)* issuing the report.

2a. REPORT SECURITY CLASSIFICATION: Enter the overall security classification of the report. Indicate whether "Restricted Data" is included. Marking is to be in accordance with appropriate security regulations.

2b. GROUP: Automatic downgrading is specified in DoD Directive 5200.10 and Armed Forces Industrial Manual. Enter the group number. Also, when applicable, show that optional markings have been used for Group 3 and Group 4 as authorized.

3. REPORT TITLE: Enter the complete report title in all capital letters. Titles in all cases should be unclassified. If a meaningful title cannot be selected without classification, show title classification in all capitals in parenthesis immediately following the title.

4. DESCRIPTIVE NOTES: If appropriate, enter the type of report, e.g., interim, progress, summary, annual, or final. Give the inclusive dates when a specific reporting period is covered.

5. AUTHOR(S): Enter the name(s) of author(s) as shown on or in the report. Enter last name, first name, middle initial. If military, show rank and branch of service. The name of the principal author is an absolute minimum requirement.

6. REPORT DATE: Enter the date of the report as day, month, year; or month, year. If more than one date appears on the report, use date of publication.

7a. TOTAL NUMBER OF PAGES: The total page count should follow normal pagination procedures, i.e., enter the number of pages containing information.

7b. NUMBER OF REFERENCES: Enter the total number of references cited in the report.

8a. CONTRACT OR GRANT NUMBER: If appropriate, enter the applicable number of the contract or grant under which the report was written.

8b, 8c, & 8d. PROJECT NUMBER: Enter the appropriate military department identification, such as project number, subproject number, system numbers, task number, etc.

9a. ORIGINATOR'S REPORT NUMBER(S): Enter the official report number by which the document will be identified and controlled by the originating activity. This number must be unique to this report.

9b. OTHER REPORT NUMBER(S): If the report has been assigned any other report numbers *(either by the originator or by the sponsor)*, also enter this number(s).

10. AVAILABILITY/LIMITATION NOTICES: Enter any limitations on further dissemination of the report, other than those imposed by security classification, using standard statements such as:

(1) "Qualified requesters may obtain copies of this report from DDC."

(2) "Foreign announcement and dissemination of this report by DDC is not authorized."

(3) "U. S. Government agencies may obtain copies of this report directly from DDC. Other qualified DDC users shall request through _____."

(4) "U. S. military agencies may obtain copies of this report directly from DDC. Other qualified users shall request through _____."

(5) "All distribution of this report is controlled. Qualified DDC users shall request through _____."

If the report has been furnished to the Office of Technical Services, Department of Commerce, for sale to the public, indicate this fact and enter the price, if known.

11. SUPPLEMENTARY NOTES: Use for additional explanatory notes.

12. SPONSORING MILITARY ACTIVITY: Enter the name of the departmental project office or laboratory sponsoring *(paying for)* the research and development. Include address.

13. ABSTRACT: Enter an abstract giving a brief and factual summary of the document indicative of the report, even though it may also appear elsewhere in the body of the technical report. If additional space is required, a continuation sheet shall be attached.

It is highly desirable that the abstract of classified reports be unclassified. Each paragraph of the abstract shall end with an indication of the military security classification of the information in the paragraph, represented as *(TS)*, *(S)*, *(C)*, or *(U)*.

There is no limitation on the length of the abstract. However, the suggested length is from 150 to 225 words.

14. KEY WORDS: Key words are technically meaningful terms or short phrases that characterize a report and may be used as index entries for cataloging the report. Key words must be selected so that no security classification is required. Identifiers, such as equipment model designation, trade name, military project code name, geographic location, may be used as key words but will be followed by an indication of technical context. The assignment of links, rules, and weights is optional.

Unclassified

Security Classification

RM 35055

CRACK EXTENSION AND ARREST: THEORY AND EXPERIMENTS FOR CONTACT STRESS FIELDS

Technical Report #5, October 15, 1975

Westinghouse Electric Corporation
Research and Development Center

Contract Number N00014-74-C-0284

Sponsored by the Advanced Projects Agency
ARPA Order Number 2697
Program Code Number 01269

Scientific Officer: Dr. A. M. Diness
Office of Naval Research

Principal Investigator: Dr. F. F. Lange
(412) 256-3684

Effective Date of Contract: April 1, 1974

Contract Expiration Date: June 30, 1976

Amount of Contract: $159,892

Form Approved, Budget -- No. 22-R0293

October 15, 1975

CRACK EXTENSION AND ARREST: THEORY AND EXPERIMENTS FOR CONTACT STRESS FIELDS

F. F. Lange
Materials Science Section
METALLURGY AND METALS PROCESSING DEPARTMENT
Westinghouse Research Laboratories
Pittsburgh, Pennsylvania 15235

ABSTRACT

No. 5 Sudden crack extension and arrest is observed when indenters are pressed into the surface of brittle materials. The energitics of this system is examined to determine the criteria for crack extension and arrest. Crack extension is defined by a condition of decreased free energy (after A. A. Griffith) and crack arrest is defined by a condition of increased free energy. The analysis results in two criteria for crack extension. First, a criterion concerning the size of the stress field must be satisfied. This size effect criterion explains the empirical Auerbach's Law which shows that the apparent strength of a brittle material increases with the decreasing size of the contact stress field. Second, a criterion concerning the crack size-maximum tensile stress must be satisfied. Once these two criteria are satisfied, a pre-existing crack will extend and then it will arrest. The size of the arrested crack is related to the size of the pre-existing crack. Experimental observations are presented to confirm the first criterion of crack extension and its relation to material properties. The experiments were performed on hot-pressed Si_3N_4 and SiC.

1. INTRODUCTION

From a thermodynamic viewpoint, crack extension will only occur when the change in free energy of a cracked body and loading system is equal or less than zero as originally defined by Griffith. To illustrate this criterion, consider the energy (U) expression for the penny-shaped crack in an infinite body as determined by Sack:[1]

$$U = 2\pi c^2 \gamma - \frac{8\sigma^2 c^3 (1-\mu^2)}{3E} ,$$

where γ = surface (or fracture) energy, c = crack length, σ = applied stress and, E, μ are the elastic constants of the body. As schematically illustrated in Fig. 1, Griffiths criterion for crack extension is satisfied when the maximum in the U vs c function coincides with the size of the pre-existing crack. As illustrated, this maximum (defined by $\frac{dU}{dc} = 0$ and $\frac{d^2U}{dc^2} < 0$) shifts to lower values of c as the stress is increased. When the maximum is shifted to coincide with the size of the pre-existing crack (in this case c_c), the free energy of the system can decrease by crack extension. Once this condition is satisfied for the above energy expression, crack extension is catastrophic because $\frac{d^2U}{dc^2}$ is always negative for larger crack sizes. The above expression negates the possibility of crack arrest because it does not include a minimum in the U vs c function (defined by $\frac{dU}{dc} = 0$ and $\frac{d^2U}{dc^2} > 0$).

The criterion for crack arrest, which is one topic of this paper, must be similar to the fundamentals for crack extension. Just as crack extension is defined by a condition of decreased free energy, crack arrest must be defined by a condition of increased free energy for further crack extension. That is, if a crack is observed to suddenly extend and then to arrest, the U vs c function must contain both a maximum and a minimum. The maximum would occur at lower crack sizes and the minimum at larger crack sizes. Their separation defines the amount of allowable crack extension.

Sudden crack extension and arrest is a common observation, e.g., the thermal cracking of brittle materials. The subject of this paper, viz., crack extension and arrest in contact stress fields, is less common but it is important to the fields of erosion and ballistic impact, surface damage inflicted to brittle materials and brittle materials bearing design.

2. CONTACT STRESS FIELDS; INTERACTION WITH BRITTLE MATERIALS

Contact stresses arise whenever two surfaces of finite radii are pressed together. A typical example is the contact stress field that

arises whenever a ball bearing is loaded onto a bearing surface. The distribution of these highly localized stresses, termed Hertzian stresses, both within the bearing and within the bearing surface volume have been well described in the literature (see, e.g., Ref. 2). Their magnitude depends on the applied load (P), the elastic properties of the material (Young's modulus, E and Poisson's Ratio, μ), and the size of the contact area (defined by the diameter D) formed between the bearing and the bearing surface. For the case where both the bearing and bearing surface materials are elastic, the size of the contact area will depend on the applied load and the elastic properties of the materials. For the case where either of the two materials exhibit plastic deformation, the size of the contact area will depend on the applied load and the yield stress of the deformable material.

The stresses of greatest concern here are those that arise in the bearing surface material caused by a spherical indenter. A triaxial state of compression exists in a tear-drop volume beneath the contact area as shown in Fig. 1a. Tensile stresses exist outside of this tear-drop shaped volume. The maximum tensile stress (σ_m) arises on and is normal to the periphery of the circular contact area:

$$\sigma_m = \frac{2(1-2\nu_b)P}{\pi D^2} \tag{1}$$

where ν_b = Poisson's ratio of the bearing material.

The interaction of contact stresses with metals and ceramics are quite different. Metals will deform in either compression or tension once their elastic limit is exceeded. Ceramics on the other hand, will not deform, but once the load reaches a critical value a large surface crack will suddenly appear at the periphery of the contact area, i.e., within the region of localized tensile stresses. It extends into the material and then arrests. Further crack extension requires an increased load. For the case of spherical indenters, the crack extends beneath the surface in the shape of a cone.

The most interesting fact concerning this cracking phenomenon, as first reported by Auerbach in 1891,[3,4] is that the calculated maximum tensile stress at which spontaneous crack extension occurs is not a constant of the material, but increases with decreasing contact area. That is, a brittle material appears stronger when smaller contact areas are used to introduce a cone crack. This phenomenon is best illustrated by the interaction of contact stresses with glass, a material with a yield stress much greater than its usually measured fracture stress. When a diamond hardness indenter is used to develop contact stresses, glasses will exhibit gross deformation prior to any cracking.[5]

The object of this article is to present a theoretical treatment and experimental data which might help to explain Auerbach Law in terms of the thermodynamics of crack extension and arrest and at the same time, direct engineers in choosing proper brittle materials to be used for applications where a high resistance to surface damage induced by contact stresses is desirable.

3. THEORY OF CRACK EXTENSION AND ARREST IN HIGH LOCALIZED STRESS FIELDS

It will be assumed that the bearing surface contains many small, pre-existing cracks and that the size of these cracks (c) are much smaller than the diameter (D) of the contact area formed with a spherical indenter, i.e., $c << D$.

If one of the pre-existing cracks, which is located at the periphery of the contact area and favorably oriented with respect to the tensile stresses, is allowed to extend into the Hertzian stress field, the initial stored strain energy U°_{SE} in both the bearing surface and the spherical indenter will be reduced due to the diminished stresses during crack extension. The strain energy associated with the contact stress field for a given normalized crack length $\mu = c/D$ can be expressed as

$$U_{SE} = U^{\circ}_{SE}\, f(\mu), \tag{2}$$

where $f(\mu)$ is a dimensionless function and by definition, $1 \geq f(\mu) \geq 0$. Roesler[6] has shown that the initial stored strain energy (U°_{SE}) in the system can be expressed as:

$$U^{\circ}_{SE} = \frac{\pi^2 k}{4(1-2\nu_b)}\, \sigma_m^{\,2}\, D^3 \tag{3}$$

where $k = \frac{1-\nu_i^{\,2}}{E_i} + \frac{1-\nu_b^{\,2}}{E_b}$ and E_i, E_b, μ_c, μ_b are the elastic moduli and Poisson's ratios of the indenter and bearing materials, respectively. Substituting Eq. (3) into Eq. (2), one obtains

$$U_{SE} = \frac{\pi^2}{4(1-2\nu_b)}\, k\, \sigma_m^{\,2}\, D^3\, f(\mu) \tag{4}$$

for the stored strain energy in the system as a function of the normalized crack depth (μ), the maximum tensile stress (σ_m) and the contact area diameter (D).

The energy required to create the new crack surfaces is

$$U_S = \gamma A, \tag{5}$$

where γ = the fracture energy of the bearing surface material and A = the surface of the crack. U_S can be expressed as a multiple of the contact area diameter ($\pi D^2/4$) as:

$$U_S = \frac{\pi}{4}\, \gamma\, D^2\, g(\mu), \tag{6}$$

where $g(\mu)$ is a dimensionless function of the normalized crack length. Again, by definition, $g(\mu) \geq 0$.

Neglecting other energy terms which are assumed not to change during crack extension, the total energy associated with the system for a given relative crack depth is

$$U_T = U_{SE} + U_S = \frac{\pi^2}{4(1-2\nu_b)}\, k\, \sigma_m^{\,2}\, D^3\, f(\mu) + \frac{\pi}{4}\, \gamma\, D^2\, g(\mu) \tag{7}$$

Using the thermodynamic criterion introduced by Griffith, crack extension will only occur when it is accompanied by a free energy change ≤ 0, i.e., for an unstable extension of the normalized crack considered here,

$$\frac{dU_T}{d\mu} = \frac{\pi^2}{4(1-2\nu_b)} k \sigma_m^2 D^3 f'(\mu) + \frac{\pi}{4} \gamma D^2 g'(\mu) \leq 0, \qquad (8)$$

This condition must correspond to a maximum in the U_T vs μ curve where $d^2U_T/d\mu^2 < 0$. Likewise, crack arrest will occur when $dU_T/d\mu = 0$ and $d^2U_T/d\mu^2 > 0$. This corresponds to a minimum in the U_T vs μ curve. A third condition may also exist where the U_T vs μ curve exhibits neither a maximum nor a minimum point, but only a single inflection. This arises where $dU_T/d\mu = 0$ and $d^2U_T/d\mu^2 = 0$.

Up to this point, no assumptions have been made concerning the specific functional forms of either $f(\mu)$ or $g(\mu)$. It is beyond the scope of this article to derive their explicit forms. For example, $f(\mu)$ would require knowledge of the stress redistribution during crack extension, which might require a numerical (e.g., finite element) stress analysis. Without going into the details, the general forms of $f(\mu)$ and $g(\mu)$ can be indicated in order to draw important conclusions from the previous analysis.

The function $g(\mu)$ is the fractional increase in the surface area during crack extension. Since it is observed that the area of the Hertzian cone crack increases during crack extension, the function $g(\mu)$ will not possess an inflection point, viz., $g'(\mu) \geq 0$ and $g''(\mu) \geq 0$ (' and '' denote first and second derivatives with respect to μ).

The function $f(\mu)$ is defined as the fractional release of stored strain-energy during crack extension. By definition $f'(\mu)$ is always < 0, i.e., at no point during crack extension can the stored strain energy be regained. In order for the U_T vs μ curve to satisfy the observed cracking phenomenon for contact stresses, viz., catastrophic extension at P_c and crack arrest, it can be shown[7] that $f(\mu)$ must possess at least one

inflection point.* This implied property of $f(\mu)$ allows the U_T vs μ function to possess both a maximum and minimum position which respectively relates to conditions where the crack size is large enough for extension and then becomes too large and must arrest.

The implication that $f(\mu)$ possesses a single inflection also means that there exists conditions where the U_T vs μ function only exhibits a single inflection without either a maximum or a minimum. As stated above, this condition occurs when $dU_T/d\mu = 0$ and $dU_T^2/d\mu^2 = 0$. By determining the first and second derivatives of U_T with respect to μ, it can be seen that the U_T vs μ curve will only possess a single inflection when

$$\sigma_m^2 D \leq \frac{\gamma}{\pi k(1-2\nu_b)} H(\mu_o) \qquad (9)$$

where $H(\mu_o) = - g'(\mu_o)/f'(\mu_o) = - g''(\mu_o)/f''(\mu_o)$ and μ_o defines the inflection point. Equation (9) is the limiting condition where crack extension will not occur regardless of the size of the pre-existing crack. Since the right hand side of Eq. (9) is a constant for a given bearing-indenter material couple, the first condition that must be satisfied for crack extension is that

$$\sigma_m^2 D \geq \text{constant} \; . \qquad (10)$$

It can be shown that Eq. (10) is equivalent to Auerbach's Law.**

As schematically illustrated in Fig. 3, once the first condition for crack extension given by Eq. (10) is satisfied, the U_T vs μ curve

---

* This assumption is based on the observed mechanics of sudden crack extension and arrest for Hertzian cracks. If $f(\mu)$ did not possess an inflection, the U_T vs μ function would only have a minimum position and it could not be used to explain the experimental observation of sudden crack extension.

** It has been shown (e.g., Ref. 3) that Auerbach's Law is only valid in the range of small contact areas (i.e., small D). Above a certain size D, the apparent strength (σ_m) is independent of the contact area size. Equation (10) shows that as $D \to 0$, $\sigma_m \to \infty$ as observed for Auerbach's Law; but as $D \to \infty$, the apparent strength (σ_m) of the material cannot $\to 0$. That is, although the strength of a brittle material depends on the volume placed under tensile stress due to the statistical nature of flaw distributions, its strength must have a finite value (σ_t) as, for example, determined by a tensile test. Thus, Eq. (1) is only valid where $\sigma_m \geq \sigma_t$.

will possess a maximum and a minimum point with increasing $\sigma_m^2 D$ corresponding to values of μ where crack extension and crack arrest will occur. By examining Eq. (7), the maximum and minimum will shift to lower and higher values of μ, respectively as the product $\sigma_m^2 D$ is increased. Thus, once Eq. (10) is satisfied, the size of the pre-existing crack, μ_c, will determine the value of $\sigma_m^2 D$ where crack instability will occur and it will also govern the final length of the stable crack.

It has been shown that two conditions are required for crack extension. First, the product $\sigma_m^2 D$ must be greater than a given value which depends on the elastic properties of the bearing and indenter materials and the fracture energy (γ) of the bearing material. Second, once this condition is satisfied, crack extension will occur when the maximum in the U_T vs μ is shifted by increasing the value of $\sigma_m^2 D$ to the value μ_c defined by the size of the pre-existing crack. At this value, the crack will extend until its normalized size reaches the minimum position in the U_T vs μ curve. Between these two values of μ, the condition for unstable crack extension ($dU_T/d\mu \leq 0$) is maintained.

4. EXPERIMENTAL OBSERVATIONS

Equation (10) predicts that a brittle material's resistance to crack extension due to contact stresses will be directly proportional to its fracture energy, γ. It also justifies, on thermodynamical reasoning, Auerbach's Law, viz., that brittle materials appear stronger when smaller contact areas are used to transfer loads.

In order to obtain insight into the validity of these predictions, contact experiments were performed on three materials, viz., hot-pressed Si_3N_4 (Norton HS-130), hot-pressed SiC (Norton Co.) and glass (soda-lime silica, Fisher microscope slides). The first two materials are promising candidates for high temperature structural applications and bearing applications. Glass, the third material, was used because its transparency

was important in verifying the relation between the presence of Hertzian cracks and the acoustic emission response used to determine P_c. As reported elsewhere, the fracture energies of hot-pressed Si_3N_4 and SiC are 45 J/m^2 and 22 J/m^2, respectively.[8] Although not directly measured for these experiments, the fracture energy for various glasses are $\sim$ 3 J/m^2.[9]

The contact experiments were conducted as follows. Similar size blocks ($\sim$ 1.5 x 2.5 x 2.5 cms) of both Si_3N_4 and SiC were diamond cut from much larger blocks purchased from the Norton Co. Flexural strength measurements previously performed on bar specimens cut from the same larger blocks were similar for both materials:[8] Si_3N_4 (weak direction): 540 MN/m^2, and SiC: 570 MN/m^2. Each of the two blocks were surface finished with a 320 grit diamond grinding wheel so that the surface damage (size and distribution of cracks) were presumably the same. Since the glass microscope slides were only used to justify an experimental procedure described below, they were used without any surface grinding.

Steel ball bearings and tungsten carbide spheres were used as indenters. Initial experiments showed that Al_2O_3 single crystal spheres were unsuitable since they would crack prior to the introduction of cracks into the Si_3N_4 bearing surface. Both the steel and tungsten carbide (cemented with cobalt) were observed to deform at loads required to introduce cracks into either Si_3N_4 or SiC. Both indenter materials were elastic in the load range required to introduce cone cracks into the glass. Different size indenters, ranging from 0.159 to 0.635 cm, were used to obtain different contact areas. Tungsten carbide spheres (0.159 cm diameter) were required to obtain the smallest contact areas for the Si_3N_4 since steel spheres of this size flattened without introducing cracks.

A load was applied with the moving crosshead (0.005 cm/min) of an Instron testing machine to the spherical indenter which was in contact with the bearing surface. Thick brass plates separated the bearing block from the load cell and the spherical indenter from the

moving crosshead. Rubber pads were also used as acoustic dampers since an acoustic emission technique was used to detect the introduction of a crack into the bearing surface.

A peizoelectric detector was mounted on the brass block in contact with the spherical indenter. The sensitivity of the electronics used to amplify the emission was set to eliminate background noise. Proof that an emission signal corresponded to the introduction of a Hertzian cone crack was obtained by observing numerous surfaces of the glass specimens just prior and after the application of the critical load required to introduce the crack. The Hertzian crack was only observed after an emission signal had been recorded. Thus as the indenter was loaded onto the bearing surface, the critical load required to introduce the cone crack was identified by the acoustic emission signal.

After each experiment, the flat surface on the spherical indenter, caused by plastic deformation, was photographed through a microscope to allow a more accurate measurement of the contact area diameter, D. As previously shown,[10] this flat area was the same size as the ring crack observed on the bearing surface of Si_3N_4 and SiC. A new indenter and a different area of the bearing surface was used for each successive experiment.

Equation (1) was used to calculate the maximum tensile stress (σ_m) required to introduce the Hertzian crack in each experiment. As suggested by Eq. (10), σ_m^2 was plotted as a function of 1/D for each of the three materials. This is illustrated in Fig. 4.

5. DISCUSSION

Figure 4 illustrates that the tensile stress required to introduce surface cracks into each material increases with decreasing contact area diameter. For the smaller contact areas, these stresses are up to

5-6 times the material's strength as measured by flexural testing of bar specimens. This figure also illustrates that a linear line can be drawn through the data for each material as predicted by Eq. (10). Best agreement for this type of plot was obtained for SiC due to the greater variation in the contact diameters obtained during testing and the smaller amount of scatter in data.

Also predicted by Eq. (10) and observed is that the relative slopes of the three sets of data are in relative agreement with the fracture energies of the three respective bearing surface materials. Best agreement was obtained for the relative slopes of the Si_3N_4 and SiC data. The ratio of these slopes is 1.9 which corresponds well to the ratio of their fracture energies, 2.0. The agreement between the glass and the two other materials is not as good. This may be due to the much lower elastic modulus of glass which should also be included in Eq. (10), the phenomenon of slow crack growth that occurs in glass which would, in effect, lower its fracture energy and the different surface finish for this material relative to the two other materials.

ACKNOWLEDGMENT

This work was supported by the Office of Naval Research under Contract No. N00014-68-C-0323.

LIST OF FIGURES

REFERENCES

1. R. A. Sack, Phil. Trans. Roy. Soc. (Lon.) 58, 729 (1946).

2. F. C. Frank and B. R. Lawn, Proc. Roy. Soc. 299a, 291 (1967).

3. F. Auerbach, Ann. Phys. Chem. 43, 61 (1891).

4. J. P. A. Tillett, Proc. Phys. Soc. 69B, 47 (1956).

5. E. W. Taylor, Nature 163, 323 (1949); J. Soc. Glass Technol. 34, 69T (1950).

6. F. C. Roesler, Proc. Phys. Soc. 69B, 55 (1956).

7. F. F. Lange, Fracture Mech. of Ceramics, Vol. 2, ed. by Bradt, Hasselman and Lange, p. 599, Plenum (1974).

8. F. F. Lange, Ann. Rev. Mat. Sci., Vol. 4, ed. by Huggins, Bube and Roberts, p. 365, Annual Reviews Inc. (1974).

9. S. M. Wiederhorn, J. Amer. Ceram. Soc. 52, 99 (1969).

10. F. F. Lange, "Task III: Relative Resistance of Dense Si_3N_4 and SiC to Surface Damage Introduced by Hertzian Contact Stresses", NAVAIR Final Rept., April 15, 1973, Contract No. N00019-72-C-0278.

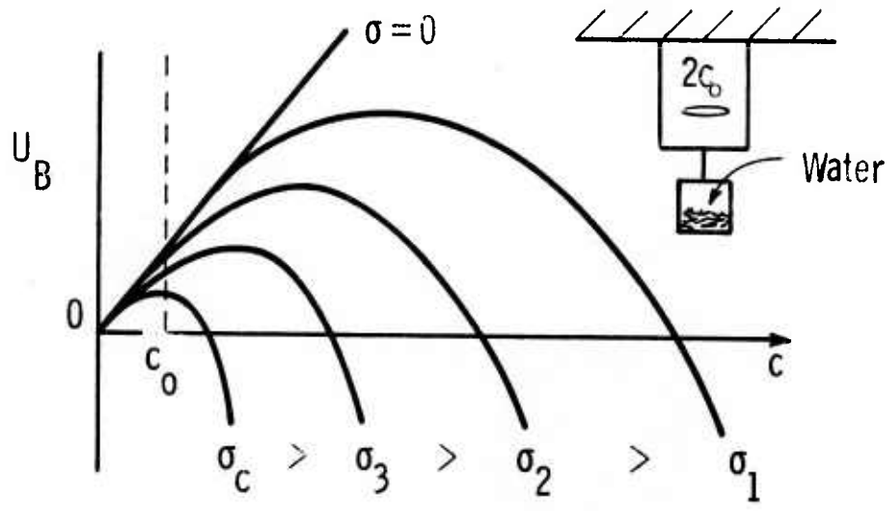

Fig. 1

Dwg. 6204A84

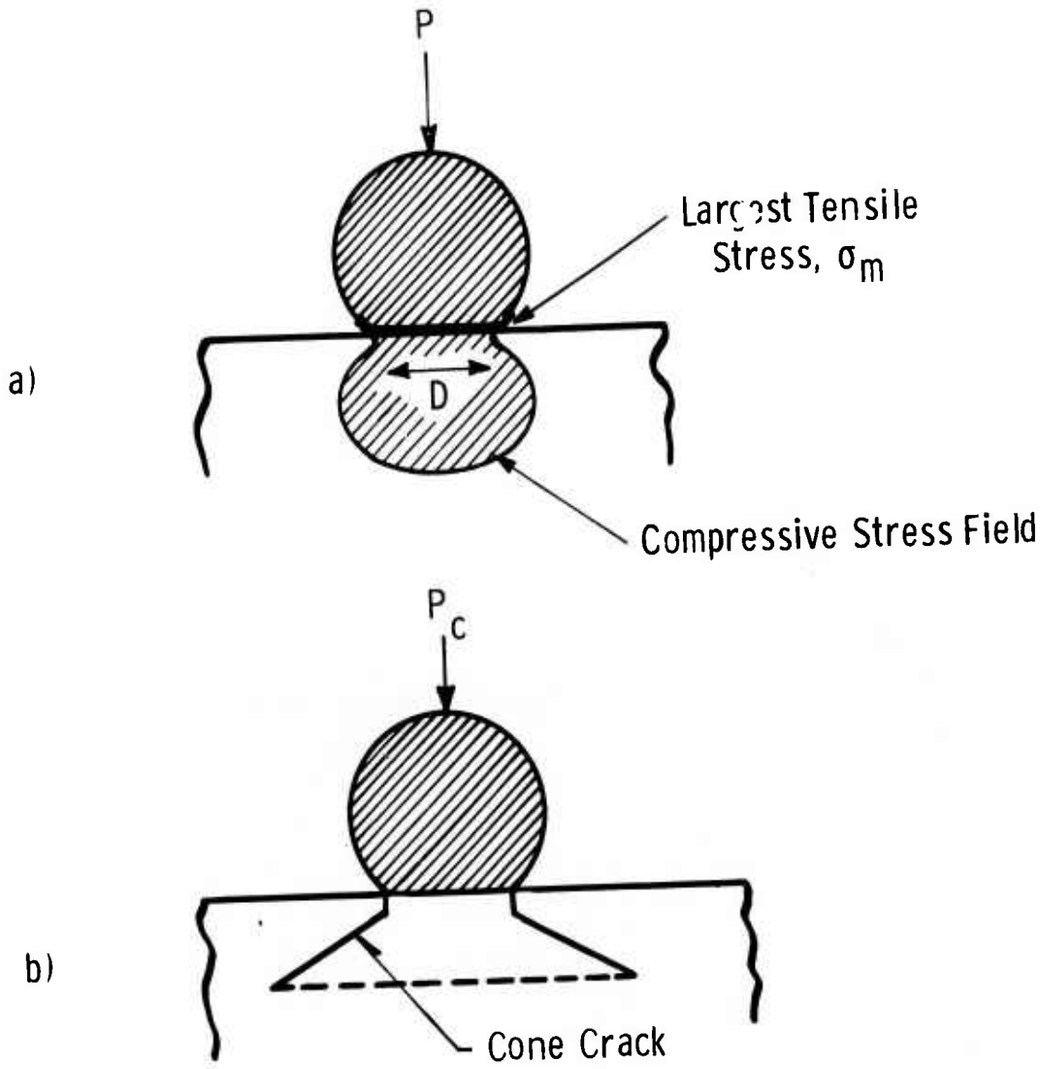

Fig. 2

Curve 677490-A

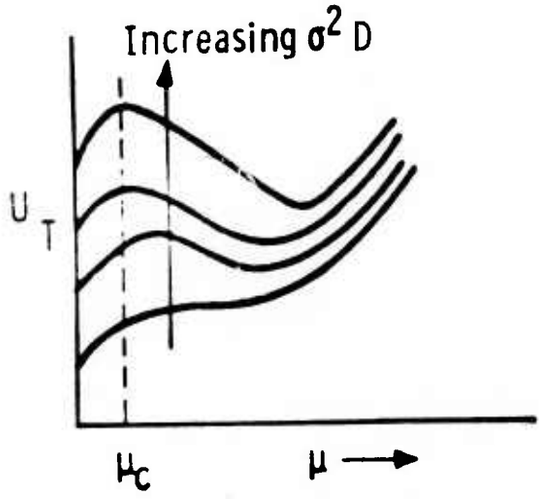

Fig. 3

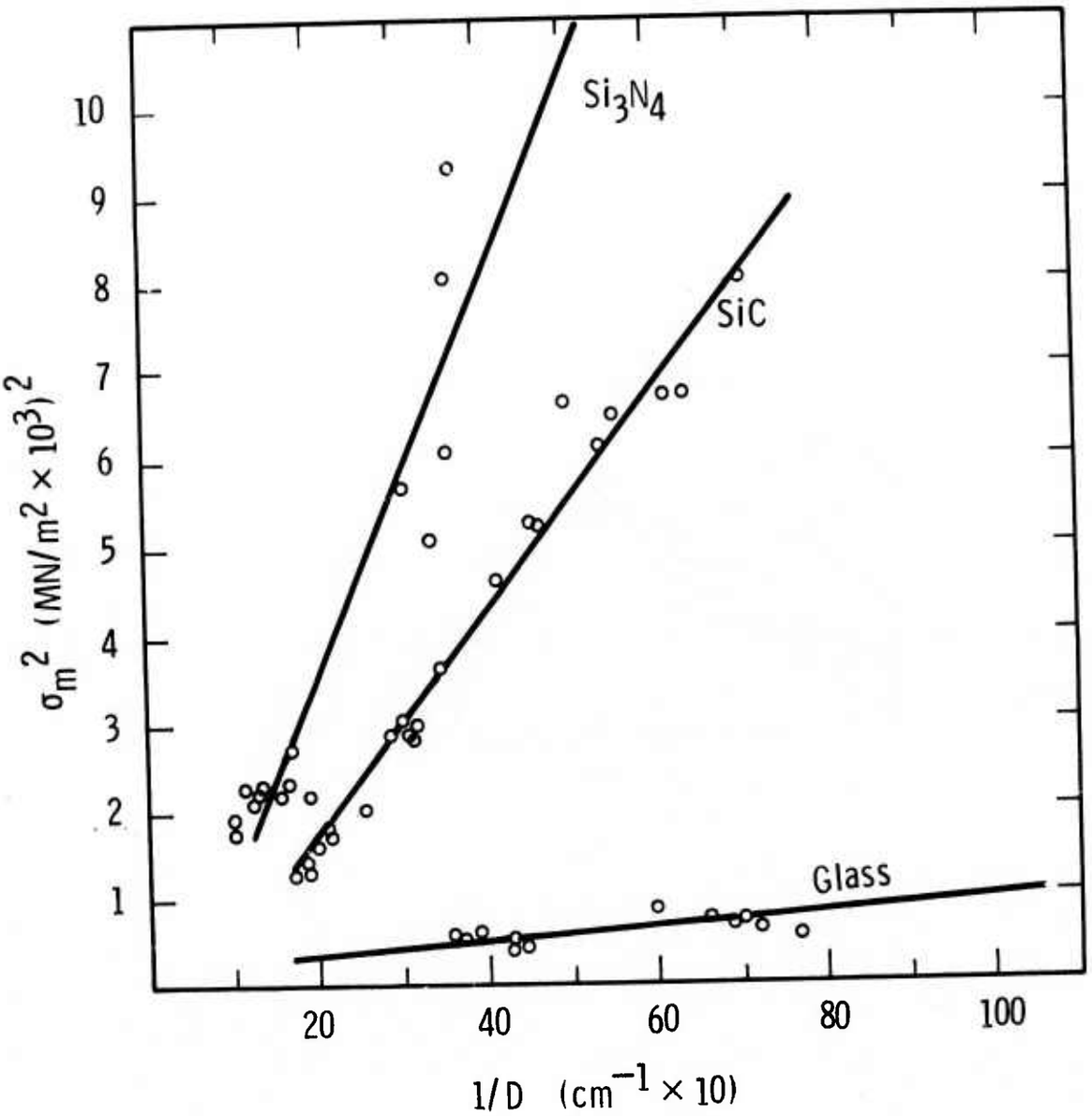
Si_3N_4
SiC
Glass
σ_m^2 $(MN/m^2 \times 10^3)^2$
1/D $(cm^{-1} \times 10)$
10
9
8
7
6
5
4
3
2
1
20
40
60
80
100

Fig. 4

Unclassified

Security Classification

#5

DOCUMENT CONTROL DATA - R&D

(Security classification of title, body of abstract and indexing annotation must be entered when the overall report is classified)

1 ORIGINATING ACTIVITY (Corporate author)

Westinghouse Research & Development Center
Pittsburgh, PA 15235

2a REPORT SECURITY CLASSIFICATION

Unclassified

2b GROUP

3 REPORT TITLE

CRACK EXTENSION AND ARREST: THEORY AND EXPERIMENTS FOR CONTACT STRESS FIELDS

4 DESCRIPTIVE NOTES (Type of report and inclusive dates)

5 AUTHOR(S) (Last name, first name, initial)

Lange, F. F.

6 REPORT DATE	7a. TOTAL NO. OF PAGES	7b. NO. OF REFS
October 15, 1975		

8a CONTRACT OR GRANT NO.	9a. ORIGINATOR'S REPORT NUMBER(S)
N00014-74-C-0284	
b. PROJECT NO.	
c.	9b. OTHER REPORT NO(S) (Any other numbers that may be assigned this report)
d.	None

10. AVAILABILITY/LIMITATION NOTICES

Reproduction in whole or in part is permitted for any purpose of the U. S. Government. Distribution of this document is UNLIMITED.

11. SUPPLEMENTARY NOTES	12. SPONSORING MILITARY ACTIVITY
	Advanced Research Projects Agency

13. ABSTRACT

Sudden crack extension and arrest is observed when indenters are pressed into the surface of brittle materials. The energitics of this system is examined to determine the criteria for crack extension and arrest. Crack extension is defined by a condition of decreased free energy (after A. A. Griffith) and crack arrest is defined by a condition of increased free energy. The analysis results in two criteria for crack extension. First, a criterion concerning the size of the stress field must be satisfied. This size effect criterion explains the empirical Auerbach's Law which shows that the apparent strength of a brittle material increases with the decreasing size of the contact stress field. Second, a criterion concerning the crack size-maximum tensile stress must be satisfied. Once these two criteria are satisfied, a pre-existing crack will extend and then it will arrest. The size of the arrested crack is related to the size of the pre-existing crack. Experimental observations are presented to confirm the first criterion of crack extension and its relation to material properties. The experiments were performed on hot-pressed Si_3N_4 and SiC.

DD FORM 1 JAN 64 1473

Unclassified

Security Classification

RM 35054

14 KEY WORDS	LINK A		LINK B		LINK C	
	ROLE	WT	ROLE	WT	ROLE	WT
contacts						
fracture						
cracks						
bearings						
silicon nitride						
silicon carbide						
stresses						
criterion						
Hertz						
extension						

INSTRUCTIONS

I. ORIGINATING ACTIVITY: Enter the name and address of the contractor, subcontractor, grantee, Department of Defense activity or other organization *(corporate author)* issuing the report.

2*a*. REPORT SECURITY CLASSIFICATION: Enter the overall security classification of the report. Indicate whether "Restricted Data" is included. Marking is to be in accordance with appropriate security regulations.

2*b*. GROUP: Automatic downgrading is specified in DoD Directive 5200.10 and Armed Forces Industrial Manual. Enter the group number. Also, when applicable, show that optional markings have been used for Group 3 and Group 4 as authorized.

3. REPORT TITLE: Enter the complete report title in all capital letters. Titles in all cases should be unclassified. If a meaningful title cannot be selected without classification, show title classification in all capitals in parenthesis immediately following the title.

4. DESCRIPTIVE NOTES: If appropriate, enter the type of report, e.g., interim, progress, summary, annual, or final. Give the inclusive dates when a specific reporting period is covered.

5. AUTHOR(S): Enter the name(s) of author(s) as shown on or in the report. Enter last name, first name, middle initial. If military, show rank and branch of service. The name of the principal author is an absolute minimum requirement.

6. REPORT DATE: Enter the date of the report as day, month, year; or month, year. If more than one date appears on the report, use date of publication.

7*a*. TOTAL NUMBER OF PAGES: The total page count should follow normal pagination procedures, i.e., enter the number of pages containing information.

7*b*. NUMBER OF REFERENCES: Enter the total number of references cited in the report.

8*a*. CONTRACT OR GRANT NUMBER: If appropriate, enter the applicable number of the contract or grant under which the report was written.

8*b*, 8*c*, & 8*d*. PROJECT NUMBER: Enter the appropriate military department identification, such as project number, subproject number, system numbers, task number, etc.

9*a*. ORIGINATOR'S REPORT NUMBER(S): Enter the official report number by which the document will be identified and controlled by the originating activity. This number must be unique to this report.

9*b*. OTHER REPORT NUMBER(S): If the report has been assigned any other report numbers *(either by the originator or by the sponsor)*, also enter this number(s).

10. AVAILABILITY/LIMITATION NOTICES: Enter any limitations on further dissemination of the report, other than those imposed by security classification, using standard statements such as:

(1) "Qualified requesters may obtain copies of this report from DDC."

(2) "Foreign announcement and dissemination of this report by DDC is not authorized."

(3) "U. S. Government agencies may obtain copies of this report directly from DDC. Other qualified DDC users shall request through _____."

(4) "U. S. military agencies may obtain copies of this report directly from DDC. Other qualified users shall request through _____."

(5) "All distribution of this report is controlled. Qualified DDC users shall request through _____."

If the report has been furnished to the Office of Technical Services, Department of Commerce, for sale to the public, indicate this fact and enter the price, if known.

11. SUPPLEMENTARY NOTES: Use for additional explanatory notes.

12. SPONSORING MILITARY ACTIVITY: Enter the name of the departmental project office or laboratory sponsoring *(paying for)* the research and development. Include address.

13. ABSTRACT: Enter an abstract giving a brief and factual summary of the document indicative of the report, even though it may also appear elsewhere in the body of the technical report. If additional space is required, a continuation sheet shall be attached.

It is highly desirable that the abstract of classified reports be unclassified. Each paragraph of the abstract shall end with an indication of the military security classification of the information in the paragraph, represented as *(TS)*, *(S)*, *(C)*, or *(U)*.

There is no limitation on the length of the abstract. However, the suggested length is from 150 to 225 words.

14. KEY WORDS: Key words are technically meaningful terms or short phrases that characterize a report and may be used as index entries for cataloging the report. Key words must be selected so that no security classification is required. Identifiers, such as equipment model designation, trade name, military project code name, geographic location, may be used as key words but will be followed by an indication of technical context. The assignment of links, rules, and weights is optional.

DISTRIBUTION LIST

Director (2)
Advanced Research Projects Agency
1400 Wilson Boulevard
Arlington, VA 22209

ATTN: Program Management

Office of Naval Research (5)
Department of the Navy
Arlington, VA 22217

ATTN: Code 471

Director
Office of Naval Research
Branch Office
495 Summer Street
Boston, MA 02210

Commanding Officer
Office of Naval Research
New York Area Office
207 West 24th Street
New York, NY 10011

Commanding Officer
Office of Naval Research
San Francisco Area Office
50 Fell Street
San Francisco, CA 94102

Director
Office of Naval Research
Branch Office
1030 East Green Street
Pasadena, CA 91101

Commanding Officer
Naval Weapons Laboratory
Dahlgren, VA 22448

ATTN: Research Division

Commanding Officer
Naval Ordnance Laboratory
White Oak, Silver Spring, MD 20910

ATTN: Code 210

Director
Naval Research Laboratory
Washington, D.C. 20390

ATTN: Technical Information Officer, Code 2000
Code 2020
Code 6000
Code 6100
Code 6300
Code 6400
Code 2029 (ONRL)

Commander
Naval Air Systems Command
Department of the Navy
Washington, D.C. 20360

ATTN: Code AIR 320A
Code AIR 5203

Commander
Naval Ordnance Systems Command
Department of the Navy
Washington, D.C. 20360

ATTN: Code ORD 033

Commanding Officer
Naval Air Development Center
Aeronautical Materials Div.
Johnsville
Warminster, PA 18974

ATTN: Code MAM

Commander
Naval Ship Systems Command
Department of the Navy
Washington, D.C. 20360

ATTN: Code 0342

Commanding Officer
Naval Civil Engineering Laboratory
Port Hueneme, CA 93041

ATTN: Code L70

Commander
Naval Ship Engineering Center
Department of the Navy
Washington, D.C. 20360

ATTN: Code 6101

Naval Ships R&D Laboratory
Annapolis Division
Annapolis, MD 21402

ATTN: Code A800

Commanding Officer
Naval Ships R&D Center
Washington, D.C. 20007

ATTN: Code 747

U. S. Naval Postgraduate School
Monterey, CA 93940

ATTN: Dept. of Chemistry and
Material Science

Commander
Naval Weapons Center
China Lake, CA 93555

ATTN: Code 5560

Commander
Naval Undersea Warfare Center
Pasadena, CA 92152

Scientific Advisor
Commandant of the Marine Corps
Washington, D.C. 20380

ATTN: Code AX

Commanding Officer
Army Research Office, Durham
Box CM, Duke Station
Durham, NC 27706

ATTN: Metallurgy & Ceramics Div.

Office of Scientific Research
Department of the Air Force
Washington, D.C. 20333

ATTN: Solid State Div. (RPS)

National Bureau of Standards
Washington, D.C. 20234

ATTN: Metallurgy Division
Inorganic Materials Div.

Atomic Energy Commission
Washington, D.C. 20545

ATTN: Metals & Materials Branch

Argonne National Laboratory
Metallurgy Division
P. O. Box 299
Lemont, IL 60439

Dr. T. Vasilos
AVCO Corporation
Research & Advanced Development Div.
201 Lowell Street
Wilmington, MA 01887

Dr. H. A. Perry
Naval Ordnance Laboratory
Code 230
Silver Spring, MD 20910

Dr. Paul Smith
Crystals Branch, Code 6430
Naval Research Laboratory
Washington, D.C. 20390

Dr. A. R. C. Westwood
RIAS Division
Martin-Marietta Corporation
1450 South Rolling Road
Baltimore, MD 21227

Dr. R. H. Doremus
R.P.I.
Materials Engineering Dept.
Troy, NY 12181

Professor G. R. Miller
Dept. of Ceramic Engineering
University of Utah
Salt Lake City, UT 84112

Dr. T. D. Chikalla
Fuels & Materials Department
Battelle Northwest
P. O. Box 999
Richland, WA 99352

Mr. G. H. Haertling
Ceramic Division
Sandia Corp.
Albuquerque, NM 87101

Mr. I. Berman
Army Materials & Mechanics
Research Center
Watertown, MA 02171

Dr. R. N. Katz
AMMRC
Watertown, MA 02171

Professor H. A. McKinstry
Pennsylvania State University
Materials Research Laboratory
University Park, PA 16802

Professor T. A. Litovitz
Physics Department
Catholic University of America
Washington, D.C. 20017

Director (2)
Advanced Research Projects Agency
1400 Wilson Boulevard
Arlington, VA 22209

ATTN: Program Management

Dr. Harold Liebowitz
Dean of Engineering
George Washington University
Washington, D.C. 20006

Dr. H. Kirchner
Ceramic Finishing Company
P. O. Box 498
State College, PA 16801

Professor A. H. Heuer
Case Western Reserve University
University Circle
Cleveland, OH 44106

Dr. D. E. Niesz
Battelle Memorial Institute
505 King Avenue
Columbus, OH 43201

Dr. F. A. Kroger
University of Southern California
University Park
Los Angeles, CA 90007

Dr. S. M. Wiederhorn
Inorganic Materials Division
National Bureau of Standards
Washington, D.C. 20234

Dr. A. G. Evans
Rockwell International Science Center
P. O. Box 1085
1049 Camino Dos Rios
Thousand Oaks, CA 91360

Dr. Co. Hulse
United Aircraft Research Labs
United Aircraft Corporation
East Hartford, CT 06108

Stanford University
Dept. of Materials Sciences
Stanford, CA 94305

Dr. R. K. MacCrone
Dept. of Materials Engineering
Rensselaer Polytechnic Institute
Troy, NY 12181

Dr. D. C. Mattis
Belfer Graduate School of Science
Yeshiva University
New York, NY 10033

Professor R. B. Williamson
College of Engineering
University of California
Berkeley, CA 94720

Professor R. W. Bould
Department of Metallurgical
and Materials Engineering
College of Engineering
University of Florida
Gainesville, FL 32601

Professor V. S. Stubican
Department of Materials Science
Ceramic Science Section
Pennsylvania State University
University Park, PA 16802

Professor R. C. Bradt
Department of Materials Science
Ceramic Science Section
Pennsylvania State University
University Park, PA 16802

Mr. J. Marshall
DCAS District, Pittsburgh
1610-S Federal Building
1000 Liberty Avenue
Pittsburgh, PA 15222

Mr. T. H. Lauterschlager
Office of Naval Research
Arlington, VA 22217

Dr. R. C. Anderson
General Electric R&D Center
P. O. Box 8
Schenectady, NY 12301

Mr. W. A. Sanders
NASA
Lewis Research Center
Cleveland, OH 44135

Library
Stellite Division
Cabot Corporation
1020 W. Park Avenue
Kokomo, IN 46901

Dr. W. Haller
Chief, Inorganic Glass Section
National Bureau of Standards
Washington, D.C. 20234

Professor M. H. Manghnani
University of Hawaii
Hawaii Institute of Geophysics
2525 Correa Road
Honolulu, HI 96822

Director (2)
Advanced Research Projects Agency
1400 Wilson Boulevard
Arlington, VA 22209

ATTN: Program Management

Director (6)
Naval Research Laboratory
Washington, D.C. 20375

ATTN: Code 2629

Director (6)
Naval Research Laboratory
Washington, D.C. 20375

ATTN: Code 2627

Ms. Elizabeth Barrett
T/M 3417
TRW Equipment
TRW Inc.
23555 Euclid Avenue
Cleveland, OH 44117

Brookhaven National Laboratory
Technical Information Division
Upton, Long Island, NY 11973

ATTN: Research Library

Director
Metals and Ceramics Division
Oak Ridge National Laboratory
P. O. Box X
Oak Ridge, TN 37830

Los Alamos Scientific Laboratory
P. O. Box 1663
Los Alamos, NM 87544

ATTN: Report Librarian

Commanding Officer
Army Materials and Mechanics
Research Center
Watertown, MA 02172

ATTN: Res. Programs Office (AMXMR-P)

Library
Bldg. 50, Room 134
Lawrence Radiation Laboratory
Berkeley, CA 94720

Commanding Officer
Naval Underwater Systems Center
Newport, RI 02844

Aerospace Research Laboratories
Wright-Patterson AFB
Building 450
Dayton, OH 45433

Mr. Richard E. Engdahl
President
Deposits & Composites, Inc.
1821 Michael Faraday Drive
Reston, VA 22090

Defense Metals Information Center
Battelle Memorial Institute
505 King Avenue
Columbus, OH 43201

Army Electronics Command
Evans Signal Laboratory
Solid State Devices Branch
c/o Senior Navy Liaison Officer
Fort Monmouth, NJ 07703

Commanding General
Department of the Army
Frankford Arsenal
Philadelphia, PA 19137

ATTN: ORDBA-1320, 64-4

Executive Director
Materials Advisory Board
National Academy of Sciences
2101 Constitution Avenue, N.W.
Washington, D.C. 20418

NASA Headquarters
Washington, D.C. 20546

ATTN: Code RRM

Air Force Materials Lab
Wright-Patterson AFB
Dayton, OH 45433

ATTN: MAMC
MAAM

Deep Submergence Systems Project
Washington, D.C. 20360

ATTN: DSSP-00111

Army Research Office
3045 Columbia Pike
Arlington, VA 22204

ATTN: Dr. T. E. Sullivan

Department of Interior
Bureau of Mines
Washington, D.C. 20240

ATTN: Science & Engineering
Advisor

Defense Ceramics Information Center
Battelle Memorial Institute
505 King Avenue
Columbus, OH 43201

National Aeronautics & Space Adm.
Lewis Research Center
21000 Brookpark Road
Cleveland, OH 44135

ATTN: Librarian

Naval Missile Center
Materials Consultant
Code 3312-1
Point Mugu, CA 93041

Commanding Officer
Naval Weapons Center Corona Labs.
Corona, CA 91720

Commander
Naval Air Test Center
Weapons Systems Test Div. (Code 01A)
Patuxent River, MD 20670

Director
Ordnance Research Laboratory
P. O. Box 30
State College, PA 16801

Commander
Naval Undersea Warfare Center
271 Catalina Boulevard
San Diego, CA 92152

Director
Applied Physics Laboratory
Johns Hopkins University
8621 Georgia Avenue
Silver Spring, MD 20901

Director Applied Physics Laboratory
University of Washington
1013 Northeast Fortieth Street
Seattle, WA 98105

Materials Sciences Group, Code S130.1
Navy Electronics Laboratory
271 Catalina Boulevard
San Diego, CA 92152

Professor R. Roy
Materials Research Laboratory
Pennsylvania State University
University Park, PA 16802

Professor D. H. Whitmore
Department of Metallurgy
Northwestern University
Evanston, IL 60201

Professor J. A. Pask
Department of Mineral Technology
University of California
Berkeley, CA 94720

Professor D. Turnbull
Div. of Engineering & Applied Science
Harvard University
Pierce Hall
Cambridge, MA 02100

Defense Documentation Center (12)
Cameron Station
Alexandria, VA 22314

TACTEC
Battelle Memorial Institute
505 King Avenue
Columbus, OH 43201

STOIAC
Battelle Memorial Institute
505 King Avenue
Columbus, OH 43201

Professor D. P. H. Hasselman
Materials Research Center
Lehigh University, Coxe Lab.
Bethlehem, PA 18015

Professor P. E. D. Morgan
Franklin Institute Research Labs.
20th & Race Streets
Philadelphia, PA 19103

Dr. B. Wilcox
Division Director
Materials Research
National Science Foundation
Washington, D.C. 20550

Dr. R. J. Charles
General Electric Co.
Research & Development Center
Box 8
Schenectady, NY 12301

Dr. R. A. Alliegro
Norton Company
Worcester, MA 01606

Mr. A. F. McLean
Ford Motor Company
Turbine Research
20000 Rotunda Drive
Dearborn, MI 48121

Dr. H. Priest
AMMRC
Watertown, MA 02171

Mr. J. H. Paster
Business Services
Mobil Tyco Solar Energy Corp.
16 Hickory Drive
Waltham, MA 02154